ON DUSA (DUST & SAND) STORMS MODELLING AND THEIR EFFECTS ON MICROWAVE RADIO LINKS

BY

SAID ABDILLAH SAID

A Thesis Presented to the
DEANSHIP OF GRADUATE STUDIES

KING FAHD UNIVERSITY OF PETROLEUM & MINERALS

DHAHRAN, SAUDI ARABIA

In Partial Fulfillment of the
Requirements for the Degree of

MASTER OF SCIENCE

In

TELECOMMUNICATION ENGINEERING

MAY 2015

KING FAHD UNIVERSITY OF PETROLEUM & MINERALS

DHAHRAN- 31261, SAUDI ARABIA

DEANSHIP OF GRADUATE STUDIES

This thesis, written by **SAID SAID ABDILLAH** under the direction of his thesis advisor and approved by his thesis committee, has been presented and accepted by the Dean of Graduate Studies, in partial fulfillment of the requirements for the degree of **Master of Science in Telecommunication Engineering**.

Dr. Ali Ahmad Al-Shaikhi
Department Chairman

Dr. Wajih Abu Al-Saud
(*Advisor*)

Dr. Salam A. Zummo
Dean of Graduate Studies

Dr. Sheikh Shariff Iqbal
(*Member*)

2/7/15
Date

Dr. Samir AlGhadban
(*Member*)

DEDICATION

To my beloved Wife, for her support and prayers to me.

ACKNOWLEDGEMENT

I wish to express my deep appreciation and thanks to Dr. Wajih A. Abu Al-Saud, who served as my advisor, for all the support and guidance. I also appreciate his positive feedback, comments and advices throughout my research.

Due thanks also to other members of the thesis committee Dr. Sheikh Shariff Iqbal and Dr. Samir AlGhadban for their contributions and great feedbacks.

I would also like to acknowledge and thank my former advisor, Dr. Kamal Harb for his guidance and continued support throughout my masters program.

I also thank Mr. Joey Espinosa from the Optics laboratory for his cooperation in setting up some experiments at the lab.

Lastly, my thanks and gratitude to my wife for her encouragement and patience without which this work would not have been possible.

Table of Contents

Acknowledgement v

List of Figures viii

List of Tables x

Publication x

List of Acronyms xi

Abstract xii

ملخص الرسالة xiv

1. **INTRODUCTION** 1

1.1 Background 1

1.2 Motivation 1

2. **THESIS OBJECTIVES** 3

3. **LITERATURE REVIEW** 4

3.1 Soil Taxonomy and Storms Characterization 5

3.2 Complex Permittivity and Relative Humidity 9

3.3 Dust Attenuation Modeling for Earth-Satellite Links 13

3.4 Example - Effective Downlink Budget for a NIUSAT Link 17

3.4.1 NIUSAT Introduction 17

3.4.2 Effective Downlink Budget 18

4. **MODEL: HORIZONTAL EXPANSE OF THE DUST STORM** 20

4.1 Modeling of The DUSA Storms & Their Impact on Terrestrial Links. 20

4.2 Visibility Layers on the Horizontal Expanse & Attenuation 21

4.3 Simulations Results 25

5. **DUSA OUTAGE AND PLANNING** 27

5.1 Dust Storm Data Source 29

5.2 Analysis of Dust Surface Concentration Data 30
5.3 Dust Surface Concentration to Visibility Translation 36
5.4 General Dust Storm Zones for Middle East & North Africa 37
5.5 DUSA Outage Planning for Terrestrial Communications 39
6. **EXPERIMENTAL WORK** 43
6.1 Motivation for Experiment 43
6.2 Experiment Methodology 45
6.3 Experiment Tools 46
6.3.A Linearity check for the camera sensor used 48
6.4 Experiment Site 52
6.5 Observed Dust Storms 53
6.6 Data Analysis 56
6.6.A Background Noise Profile 57
6.6.B Targets Intensity Profile 57
6.6.C Analysis and Discussion 60
6.7 Limitations of the Experiment Technique 67
7. **CONCLUSION** 69
7.1 Future Work 71
REFERENCES 73
VITAE 76

List of Figures

Figure 1 - Triangular diagram of soil texture classes by the USDA. 7
Figure 2 - Map of soil grain types and sizes in the Middle East 8
Figure 3 - Variation of the permittivities with moisture content. 11
Figure 4 - Simulation results of DUSA attenuation (Earth-Satellite). 16
Figure 5 - Link Margin ITU-R (Rec. UIT-R F.1247-1). 19
Figure 6 - 3D geometrical structure of a progressing dust plume 20
Figure 7 - Simplified model of a progressing dust storm (top view) 22
Figure 8 - Output of the DUSA attenuation simulation (Terrestrial) 25
Figure 9 - A world map showing the largest arid and semi-arid regions on the globe. 28
Figure 10 - The HWSD major soil texture classes of the world's soils 28
Figure 11 - Sample dust surface concentration forecasted on 11 Feb 2015. 31
Figure 12 - Dust Surface Concentration Range 2 (5-20 µg/m³) 32
Figure 13 - Dust Surface Concentration Range 3 (20-50 µg/m³) 33
Figure 14 - Dust Surface Concentration Range 4 (50-200 µg/m³) 33
Figure 15 - Dust Surface Concentration Range 5 (200-500 µg/m³) 34
Figure 16 - Dust Surface Concentration Range 6 (500-2000 µg/m³) 34
Figure 17 - Dust Surface Concentration Range 7 (2000-5000 µg/m³) 35
Figure 18 - Dust Surface Concentration Range 8 (5000-20000 µg/m³) 35
Figure 19 - Dust Surface Concentration Range 9 (>20000 µg/m³) 36
Figure 20 - Major dust storm zones of the North Africa and Middle East. 37
Figure 21 - Translation of dust surface concentration to visibility. 39
Figure 22 - DUSA Outage: Loamy, X-band (8-12GHz), H (0%) 40
Figure 23 - DUSA Outage: Loamy, KA-band (26.5-37GHz), H(0%) 40
Figure 24 - DUSA Outage: Sandy-Loam, KA-band (26.5-37GHz), H(5%) 41
Figure 25 - DUSA Outage: SiltyClay, K-band (18-26.5GHz), H(3%) 41
Figure 26 - DUSA Outage: Sandy, X-band (8-12GHz), H(4%) 41
Figure 27 - DUSA Outage: Sandy, KU-band (12-18GHz), H(0%) 41
Figure 28 - DUSA Outage: Sandy, KU-band (12-18GHz), H(5%) 42
Figure 29 - DUSA Outage: Sandy, KA-band (26.5-37GHz), H(5%) 42
Figure 30 - Variation of visibilities on the horizontal expanse 43

Figure 31 - A dummy terrestrial network vulnerable to DUSA storms. 44
Figure 32 - Experimental setup 46
Figure 33 - The Microsoft LifeCam Cinema (H5D-00001) web camera used 47
Figure 34 - Mounting of web camera to the telescope 47
Figure 35 - Schematic of the camera sensor system. 48
Figure 36 - The digital light meter and the light source used. 49
Figure 37 - Linearity response of the light source used. 49
Figure 38 - Setup of the linearity test at optics laboratory 50
Figure 39 - The 17 captured images for linearity test 51
Figure 40 - Linearity response of the web camera used. 51
Figure 41 - Dust storm observed on 4 November 2014 in Dhahran area. 53
Figure 42 - Clear day in Dhahran 6 November 2014. 53
Figure 43 - NASA picture of the worst storm on April 2, 2015 55
Figure 44 - Schematic of the analysis methodology. 56
Figure 45 - The intensity profile for the average background noise. 57
Figure 46 - The extracted profiles of the observed storms. 58
Figure 47 - Graph - Intensity profiles for all observed dust storms 59
Figure 48 - Schematic of the experiment configuration 60
Figure 49 - Channel attenuation data for all observed DUSA storms 63
Figure 50 - DS1 channel attenuation behavior 63
Figure 51 - DS2 channel attenuation behavior 64
Figure 52 - DS3 channel attenuation behavior 64
Figure 53 - DS4 channel attenuation behavior 64
Figure 54 - Averaged attenuation over all the 4 observed dust storms 65

List of Tables

Table 1 - List of published DUSA complex permittivities. 10
Table 2 - NIUSAT considered losses (maximum values) 18
Table 3 - NIUSAT summary of downlink budget output parameters. 19
Table 4 - Summary of the major world desert regions 29
Table 5 - Overview of the studied major dust storm zones 38
Table 6 - The ETX-90 telescope specifications 46
Table 7 - The web camera specifications 48
Table 8 - Summary of observed dust storms in the Dhahran region 54
Table 9 - The extracted target intensity pixel data 58
Table 10 - Channel lengths from telescope to targets 60
Table 11 - Processed dust storm data using equations (23) and (24) 62

Publication

Harb Kamal, Abdillah Said, Abdul-Jauwad Samir, "**Dust & Sand (DUSA) Storms Impact On LEO Satellite Microwave Radio Links**," *Advanced Satellite Multimedia Systems Conference and the 13th Signal Processing for Space Communications Workshop (ASMS/SPSC), Livorno, Italy*. pp.442,447, 8-10 Sept. 2014

(*copy attached*)

List of Acronyms

ASDF	Atmospheric Sand and Dust Forecast
BDFC	Barcelona Dust Forecast Center
BSC	Base Station Controller
BTS	Base Transceiver Station
C-band	4 - 8 GHz
DAF	Dust Attenuation Factor
DS#	Dust Storm 1,2,3,4 & 5
DUSA	Dust and Sand
EIRP	Effective Isotropic Radiated Power
FREQ.	Frequency
GA	Gaseous Attenuation
GSM	Global System for Mobile Communications
HWSD	Harmonized World Soil Database
IPL	International Private Line
ITU-R	International Telecommunication Union Radiocommunication
KA-band	26.5 - 40 GHz
KFUPM	King Fahd University of Petroleum & Minerals
KU-band	12 - 18 GHz
LEO	Low Earth Orbit (Altitude range 160 - 2000 Km)
MWiFS	Miniature Wide Field Sensor
NA-ME-E	Northern Africa-Middle East-Europe
NANOSAT	Nano Satellite (Miniaturized with wet mass between 1-10Kg)
NASA	National Aeronautics and Space Administration
NIUSAT	Noorul-Islam University Satellite
PSD	Particle Size Distribution
QOS	Quality of Service
QPSK	Quadrature Phase Shift Keying
S-band	2 - 4 GHz
SDS-WAS	Sand and Dust Storm Warning and Assessment System
SNR	Signal-to-Noise Ratio
TLI_C	Target Light Intensity during Clear day
TLI_D	Target Light Intensity during Dust storm
USDA	United States Department of Agriculture
USNCSS	United States National Cooperative Soil Survey
WMO	World Meteorological Organization

Abstract

Full Name : SAID ABDILLAH SAID

Thesis Title : On DUSA (Dust & Sand) Storms Modelling & Their Effects On Microwave Radio Links

Major Field : Telecommunications

Date of Degree : May 2015

Wireless communication today is increasingly becoming an integral part of our daily lives. Research and discoveries in this field have continuously improved the communication experience and service. Numerous challenges though are still encountered as telecommunication service providers try to keep up with quality of service (QoS) levels in a highly competitive market. Dust and sand (DUSA) storms in arid and semi-arid regions continuously pose a looming threat to microwave radio systems operation and reliability. For an earth-satellite link scenario, a novel technique is adopted to model the dust storm in which the fundamental variables defining the storm, such as the average dust particles size, visibility and storm height are compounded in a unified formulation. A real downlink improvement for a miniaturized LEO satellite will be redesigned by considering the dust attenuation parameter from the model. Moreover, a novel idea of visibility layering is introduced on the horizontal expanse of the storm, remodeling it for better attenuation prediction in terrestrial radio systems. Additionally an analysis of DUSA outage and its planning is also presented for two most dust prone regions of the world with the aim of helping system engineers design and estimate link budgets for terrestrial microwave communications. This study will also encompass experimental work investigating the physical model of the dust storm, particularly the

visibility layers on the horizontal expanse of the storm and their effect on wireless communication. This investigation will shade more light on the storm's complex structure in the hope that it will lead to a more accurate, efficient attenuation computation and its mitigation, ultimately resulting in perfection of radio link design.

ملخص الرسالة

الاسم الكامل: سعيد عبدالله سعيد

عنوان الرسالة: نمزجه الغبار والعواصف الرملية وتأثيرها على وصلات المايكروويف

التخصص: الاتصالات السلكية واللاسلكية

تاريخ الدرجة العلمية: مايو (أيار) 2015

الاتصالات اللاسلكية على نحو متزايد يعتبر جزءا لا يتجزأ من حياتنا اليومية. إن الأبحاث والاكتشافات في هذا المجال قد تحسنت بشكل مستمر في عملية تجربة خدمات الاتصالات. وعلى الرغم من التحديات العديدة التي لا يزال يواجهها مقدمي خدمات الاتصالات السلكية واللاسلكية مواكبة تستدعي مستويات مدروسة للحفاظ على جودة الخدمة بوجود سوق تنافسية عالية.

العواصف الترابية والرملية في المناطق القاحلة وشبه القاحلة تشكل باستمرار خطرا يلوح في الأفق لتشغيل الأنظمة الراديوية والميكروويف بشكل سليم. وللحصول على رابط السيناريو مع قنوات فضائية الأرض، تم اعتماد تقنية جديدة لتمثيل العاصفة الترابية التي تتفاقم مع المتغيرات الأساسية التي تحدد العاصفة مثل متوسط حجم جزيئات الغبار، والرؤية وارتفاع العاصفة في صياغة موحدة.

ولذلك سيتم إعادة تصميم وتحسين الهابطة الحقيقي لمدار القمر الاصطناعي المنخفض (LEO) من خلال النظر في تخفيف الغبار من النموذج. وعلاوة على ذلك، هو عرض فكرة جديدة لوضوح الرؤية بشكل طبقات أفقية على امتداد للعاصفة، وإعادة عرض لتحسين التنبؤ بقوة الموجة في الأنظمة الأرضية للراديو.

هذه الدراسة تشمل أيضا تحقيق العمل التجريبي في النموذج التركيبي للعاصفة الترابية، ولا سيما طبقات الرؤية الأفقية على فسحة من العاصفة وتأثيرها على الاتصالات اللاسلكية. من هنا سوف نسلط المزيد من الضوء على بنية العاصفة المعقد على أمل أن يؤدي ذلك إلى أكثر دقة وكفاءة حساب التأثير على قوة الموجة والتخفيف من آثارها، مما ينتج في نهاية المطاف إلى إكمال تصميم وصلة الراديو.

1. Introduction

1.1. Background

Scientific findings have lately revealed that atmospheric dust and sand (DUSA) blowing off from vast central African deserts and the Middle East to the basin of the Amazon compensates for poor rainforest soils [1]. As the DUSA plumes nourish the ecological systems of the world, they concomitantly pose a big threat to wireless communication systems, both terrestrial and satellite, by hampering them through degradation of the microwaves. Other meteorological circumstances similarly play a significant role in causing propagation impairments on microwave systems. Severe cases can cause total radio link unavailability [2]. Ensuring standards of the Quality of Service (QoS), it is necessary for engineers to come up with effective solutions that can better predict, estimate and compensate for all possible radio link degraders in the free space channel.

1.2. Motivation

The microwave spectrum containing wireless and satellite networks for broadband multimedia communications are being extensively deployed all over the world. This has motivated a lot of research in designing efficient microwave communication systems. The focus has been on the free-space channel and understanding the effects in terms of signal attenuation due to rain, snow, sand and dust (DUSA) present at some point along the free-space channel depending on region of operation. The scenarios get worse as higher frequency bands are approached and beyond their ambit.

For Arid and semi-arid regions like the Middle East and North Africa which frequently experience DUSA storms, terrestrial and satellite microwave systems in these regions

will be affected to a certain level due to different dust related parameters such as particle sizes , their distribution, visibility, composites and relative humidity level during the storms. Since these parameters keep varying from region to region, it is a big challenge to come up with a generic model of this complex phenomenon. The methodologies to properly relate all these parameters together is an even more challenging issue.

2. Thesis Objectives

The main goal of this work is to try to understand the physical model of dust and sand storms and their impacts on microwave radio links both satellite and terrestrial. Some of the major areas touched in this thesis work are as below:

a) An extensive literature review understanding the current methods to quantify the dust and sand storms impacts on microwave radio communications. Particular areas of interest include but are not limited to Soil taxonomy, Permittivities & Relative Humidity effects on the dielectric properties of the particles.

b) Development of a simpler method to approximate dust storms models based on layering concept on the horizontal expanse of the storm.

c) Intuitive and conceptual formulation for the modeling modifications done using current available models in literature.

d) Redesigning of a real downlink for a NANOSAT taking in consideration the dust attenuation parameter.

e) Analysis of DUSA outage and planning for the regions of Middle East and North Africa to help system engineers design and estimate link budgets for terrestrial microwave communications.

f) Experimental measurements and investigation with regards to dust and sand storm's physical model based on variation of visibility along the horizontal expanse.

3. Literature Review

The fundamental idea of telecommunications is the transfer of a signal from a sender terminal to a receiving terminal via a medium e.g. the free space channel. The signal propagation along any medium will face threats that will lead to distortion of the signal. This will affect the signal fidelity leading to excessive digital transmission errors. Examples include satellite television reception that is affected by different atmospheric conditions like rain [3] - [4] to high priority services such as satellite data service delivered through VSATs and satellite (International Private Line) IPL platforms.

Degradation of signals entails their weakening as they travel through the channel. The channels are far from perfect. Free space, for example, is composed of numerous layers that are unidentical in their composition and structure. These layers create losses in signal propagation under different weather conditions [4]. The extent of signal interaction with the channel largely depends on the inherent characteristics of the signal, such as the carrier frequency and polarization.

Satellite communication signals in the microwave bands are a main victim when it comes to attenuation. Apart from the path loss that largely dominates the total losses faced by a satellite signal, other meteorological-related factors also contribute to the available signal to noise ratio of the system. Rain attenuation's impairment for satellite signals becomes particularly severe as the operation frequency increases. In C – band, it is not as critical as that of higher bands. However, the diameter of a raindrop is definitely detrimental for Ku and Ka – band signal passage. It is to be noted that Ku – band attenuation in rain is approximately 9 times that of C – band [4].

Efficient weather prediction systems are thus an important design factor to be considered in order to improve QoS and optimize satellite radio links [5]. This ensures that the cost of operation or leasing the links becomes manageable and practical in overcoming the restriction of increasing transmission power. Other parameters can be used to increase system's throughput and availability including modulation type, coding technique ... etc. [6].

Therefore it is important to study these meteorological effects to better stand a chance of minimizing their impacts on microwave communication systems. This will enable engineers to have better control over the SNR in their systems. The information can be used to optimally design other components of the system like antenna size, power levels and other factors in order to counteract the rain and dust storm effects.

The following sub-sections summarize the literature related to soil taxonomy, dust storms physical descriptions, complex permittivities and effects of relative humidity to the particles behavior and properties.

3.1 Soil Taxonomy and Storms Characterization

This sub-section briefly describes the physical construction of dust and sand (DUSA) storms most commonly observed in arid and semi-arid lands of the world. A number of factors can make a geographical area become prone to DUSA storms including the soil type, climate and topography [7].

The particle size distribution (PSD) in the atmosphere is critical in precise prediction of an aftermath of a storm. The soil textural class of the region involved will greatly impact

the PSD [8]. A sifting method has been used by Bagnold [9] to estimate the PSD. He found out that radius of majority of particles range between 0.08-0.15 mm. He also concluded that in a typical sand storm, majority of the particles suspended will be of radii less than 0.1 mm.

Work done in Sudan by Ghobrial [10] confirms Bagnold's figures in which they discovered that all particles had radii of less than 0.15mm and that particles with less than 0.005 mm formed more than 30% of the total particles population distributed exponentially. Ansari in [11] concluded that the maximum radius a particle in a dust storm will have is 0.1 mm.

On the other hand, the soil texture varies from region to region in the desert areas of the world. The United States Department of Agriculture (USDA) and the National Cooperative Soil Survey of the United States (USNCSS) have developed a soil taxonomy providing an elaborate classification of soil types according to several parameters and properties.

The triangular diagram in Figure 1 summarizes the descriptions of the classes.

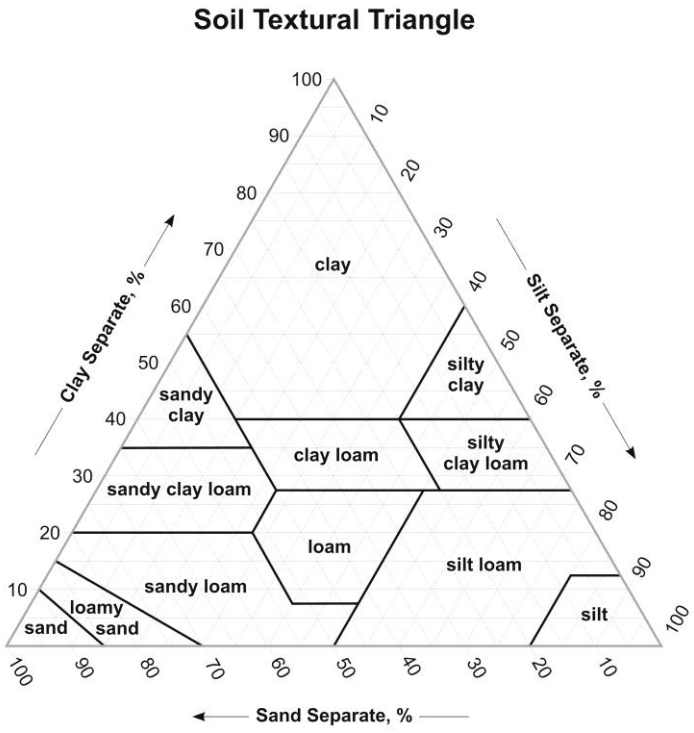

Figure 1 - Triangular diagram of soil texture classes by the United States Department of Agriculture (USDA).

In Saudi Arabia for example, dust and sand storms are experienced round the year with areas rich in silt and clay being responsible for the majority of the storms. These fine grained soils are found in areas with dry lake beds and river flood plain deposits. Figure 2 shows a map of soil grain sizes in the Arabian Peninsula. Topographically low lying regions favor dust storm generation because prevailing winds are unimpeded by higher terrain. As for climate, it is clear that the world's arid desert and semi-arid climate zones highly correlate with the major worlds deserts [7].

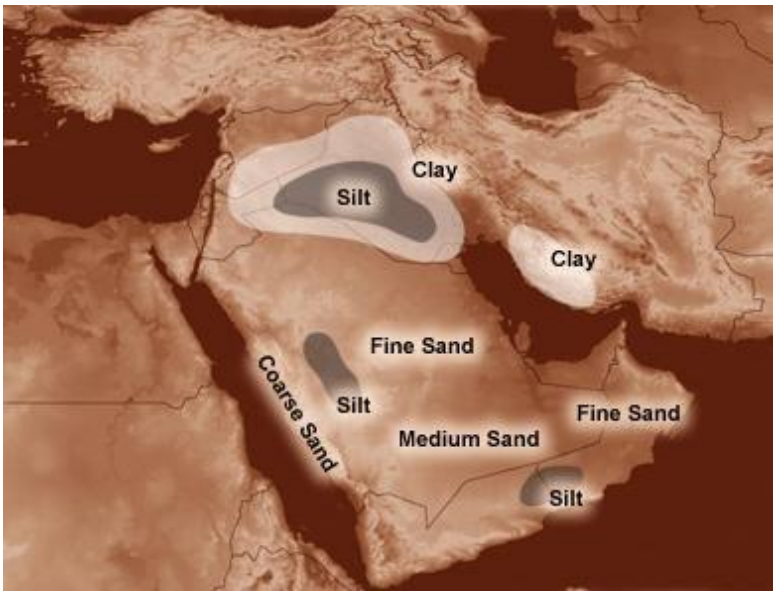

Figure 2 - Map of soil grain types and sizes in the Middle East [7].

Generally during the storms, top soil is blown up in the air. Dust particles will remain suspended in the air when upward currents are greater than the speed at which the particles fall through air. Larger particles (diameter > 80 micron) rise only few meters and have faster settling speeds once the storm is over. They settle when the wind speeds drop below the speed necessary to carry them. Zender [12] did extended work on the issue of gravitational settling for a turbulent mixture of particles. According to his work, the dust haze, mainly comprising of finer particles (diameter< 20 micron), will persist to be airborne for longer periods of time (as there settling speed is very low) at few kilometers above the ground and downstream from the source for days after the storm, hence greatly impacting earth-satellite communication links.

The visibility of a dust storm determines its classification. To be classified as a dust storm, the visibility must be smaller than 1 Km. When the visibility is shorter than 500 m, it is considered a severe dust storm [13].

3.2 Complex Permittivity and Relative Humidity

Dust and sand particles suspended in the air after a storm pose threats to microwave radio systems reliability. Knowledge of the dielectric constant of particles suspending or precipitating in the atmosphere is of importance in radio communication and radio meteorology [13]. Though several studies exist in literature on the complex permittivity of sand and dust samples have been reported, there is no precise theory existing for calculating it. Some techniques employed recently to estimate permittivity values include the resonant cavity measurement, waveguide measurements and extrapolation of their results [14].

The permittivity of materials at microwave bands is:

$$\varepsilon = \varepsilon' - j\varepsilon'' \qquad \textbf{(1)}$$

where the real part ε' is the dielectric constant and the imaginary ε'' is the dielectric loss factor. A summary of the complex dielectric constants published is shown in Table 1. These values are assumed to be the most accurate as they have been most widely cited in literature as per the survey of several geophysical research journals done by the authors in [11].

Band	**Frequency Range (*GHz*)**	**Soil Type**	**Moisture Content % (H_2O/g)**	**Dielectric Constant ($\varepsilon' - j\varepsilon''$)**	**Reported by**
S	1 - 4	Sandy	0	2.55-j0.016	Von Hippel [15]
		Soil	4	4.4-j0.2024	
			16.8	20-j2.6	
		Loamy	0	2.44-j0.003	
			2.2	3.5-j0.14	
			13.7	20-j2.4	
		Clay	0	2.20-j0.034	
			20	11.3-j2.825	
X	8 - 12	Sandy	0	2.53-j0.01	Von Hippel [15]
		Soil	3.88	3.6-j0.432	
			16.8	13-j3.77	
		Loamy	0	2.44-j0.003	
			13.7	13.8-j2.484	
Ku	12 - 18	Sandy Soil	0.3	2.8-j0.035	Njoku and Kong [16]
			5	3.9-j0.62	
			10	5.5-j1.3	
			20	9.2-j4	
			30	11.8-j7	
K	18 - 26.5	Silty Clay Loam	3	3.4-j0.2	Schmugge, Gloersen, Wilheit and Geiger [17]
			12	4.7-j1.1	
			22	13.6-j6.8	
			30	16.25-j9.25	
Ka	26.5 - 37	Sandy Soil	0.3	2.5-j0.028	Njoku and Kong [16]
			5	3.6-j0.65	
			10	5.1-j1.4	
			20	7.8-j5.3	
			30	9.8-j9.9	
		Loamy Fine Sand	0	2.53 - j0.065	
			5	2.45-j0.375	Geiger and Williams [18]
			10	4-j1.325	
			15	6.72-j3.188	
			20	7.375-j4.156	
		Sandy Clay Loam	0	2.515-j0.073	
			5	2.88-j0.353	
			10	3.290-j0.728	
			15	7.088-j3.5	
			20	8.588-j4.765	

Table 1 - List of published DUSA complex permittivities.

As can be inferred from the table, there is little variation in both real and imaginary parts for the dry soil types. Moreover, the complex permittivity also depends on frequency and moisture content [13].

In humid weather conditions, dust and sand particles in air will absorb water vapor. Measurements done by Shariff [19] in Khartoum, Sudan, showed that with 82% relative humidity in air, the dust will absorb up to 5.1% by weight moisture. This has a big impact on the dielectric constant as it increases it considerably. Sharif and Ghobrial in [20] also investigated the effect of hygroscopic water on the permittivity. Their work revealed that both parts of the permittivity increased with increasing water content. In that work they published the figure below indicating the variations of the imaginary and the real parts of the permittivity with moisture content from one of the samples they studied at a frequency of 8.3 GHz.

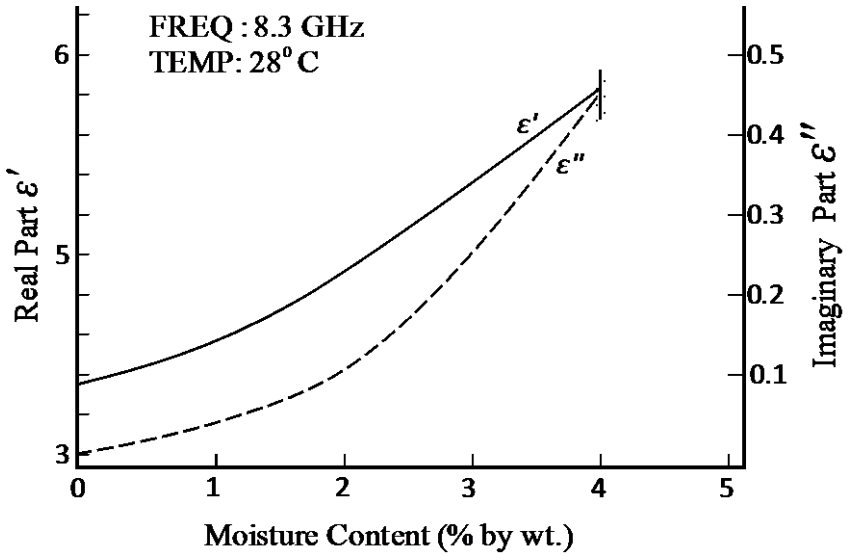

Figure 3 - Variation of the real and imaginary parts of the permittivity with moisture content done in [20].

The Gulf region experiences humid conditions especially in the coastal regions. The work done in Khartoum concluded that given any value of air relative humidity (*H%*), the new dielectric constant can be predicted by the equations (2) and (3) below:

$$\varepsilon'_H = \varepsilon' + 0.04H - 7.78 \times 10^{-4}H^2 + 5.56 \times 10^{-6}H^3 \quad \textbf{(2)}$$

$$\varepsilon''_H = \varepsilon'' + 0.02H - 3.71 \times 10^{-4}H^2 + 2.76 \times 10^{-6}H^3 \quad \textbf{(3)}$$

Where $(\varepsilon' + j\varepsilon'')$ is the dry dust dielectric permittivity.

Experimental studies done by Alhaider and Ali [21] in Riyadh, Saudi Arabia, where they observed and collected data for 9 dust and sand storms experienced during the year 1987, have shown that the measured attenuation is considerably higher than the estimated attenuation using typical sand and dust particles moisture content of up to 10%. They also concluded that moisture gained by dust particles will not exceed 10% for a relative humidity of 90% in the atmosphere.

Therefore it is without doubt that moist dust and sand particles will affect the satellite microwave links more severely than dry particles in humid areas and thus relative humidity is a necessary parameter that needs to be considered in accurate determination of satellite links degradation caused by meteorological factors.

A more recent work by Harb *et al.* in [22] presented an analytical solution to predict gaseous attenuation (GA) in dust free environments. GA was estimated by summing up the effects of all of the significant resonance lines of the gasses in air (most dominantly those from atmospheric oxygen and water vapor).

3.3 Dust Attenuation Modeling for Earth-Satellite Links

In this sub-section, a few methods of modelling dust and sand attenuation over earth-satellite links are highlighted as per previous work in literature leading to the current adoption and improvements on the modelling of this complex phenomenon.

Julius Goldhrish did extensive work in [23] to quantify the microwave attenuation for frequencies upto 40GHz under various dusty conditions. The model has also been adopted in a number of publications including [24]–[26]. The attenuation caused by the storm was determined as a function of the dielectric constant shown below:

$$A = \frac{2.317 \times 10^{-3}.\varepsilon''}{[(\varepsilon'+2)^2+\varepsilon''^2]\lambda} \cdot \frac{1}{V^{1.07}} \qquad [dB/Km] \qquad \textbf{(4)}$$

where ε' is the real part of the particles dielectric constant, ε'' is the imaginary part of the particles dielectric constant, λ is the wavelength in meters and V is the visibility in Km.

The slant path over which the radio wave propagated on was simply given as:

$$L_s = \frac{h}{\sin\theta} \qquad [km] \qquad \textbf{(5)}$$

where L_s is the slant path in Km, h is the height of the storm in Km and θ is the angle of propagation to the satellite terminal in degrees.

Thus to find the total attenuation, it would follow that one would multiply (4) and (5) together to give:

$$A_L = \frac{2.317 \times 10^{-3}.\varepsilon''}{[(\varepsilon'+2)^2+\varepsilon''^2]\lambda} \cdot \frac{1}{V^{1.07}} \times L_s \qquad [dB] \qquad \textbf{(6)}$$

The assumption here was that the microwave signal experienced an identical dusty medium throughout its path within the storm. The equation would slightly be altered to accommodate other parameters like type of dust involved (soil type) and humidity content in the atmosphere during the dust storm event.

Elsheikh and his team in [24] proposed an adjustment factor reflecting the vertical structure of the dust storms based on the previous vertical dust storm behavior. They found out that the computed attenuation on assumption that the vertical dust storm intensity is uniform was much higher and unrealistic leading to over estimation of the total attenuation. To consider the varying intensity profile of the storm, they introduced an adjustment factor given as below:

$$r_v = \frac{h_o^{0.26} \times h_i^{0.74}}{0.74 \times L \times (sin\theta)^{1.74}} \qquad \textbf{(7)}$$

where r_v is the vertical adjustment factor dependent on slant path L, dust storm height h, reference height h_o and the elevation angle θ. This consideration improved utilization of resources when compensating for attenuations in dusty weather conditions on earth-satellite links.

A further improvement on the work of Elsheikh was proposed by Harb and his team in [5]. They developed a physical model of a dust storm composed of several visibility dependent layers referenced to the non-uniform variations of height along the storm altitude. By chopping the dust storm into various layers and visibility doubling with each layer going upwards, the visibility V_i at any height h_i can be related to the visibility V_o at a certain reference height h_o by:

$$V_i = V_o \left[\frac{h_i}{h_{(i-1)}}\right]^{0.26} \quad \textbf{(8)}$$

Following the concept in [24], the slant path L is also chopped into smaller layers depending on the visibility at individual layers. Total path length will be the summation of these individual path lengths:

$$L(\theta) = L_1 + L_2 + \cdots + L_N = \sum_1^N \frac{h_i}{\sin\theta} \quad \textbf{(9)}$$

For this work, the dust attenuation parameter is simply extracted and used to redesign the downlink link budget of a real satellite link which will be discussed in the upcoming section. The following equations were used to estimate the dust attenuation:

$$A_{p_i} = \left[\frac{567}{V r_e^2 \lambda}\right]\left[\frac{\varepsilon''}{(\varepsilon'+2)^2 + \varepsilon''^2}\right]\sum_{i=1}^{N} P_i r_i^3 \quad \textbf{(10)}$$

$$A_D = \sum_{i=1}^{N} A_{p_i} \quad \textbf{(11)}$$

where A_{p_i} are the layered point attenuations in *dB/Km* at each i^{th} layer and A_D is the total attenuation in *dB*. V is the visibility in *Km* , r_e is the equivalent particle radius, λ is the operating wavelength, ε'' and ε' are the real and imaginary parts of the dielectric constants respectively, $\sum_1^N P_i r_i^3$ represents the volume summation for different probabilities of particle sizes multiplied by the cubic of the dust particle size, N is the highest layer level. Full list of published dust and sand complex permittivities is presented in Table 1.

Simulation of the equations (10) and (11) above yielded the graph shown in Figure 4:

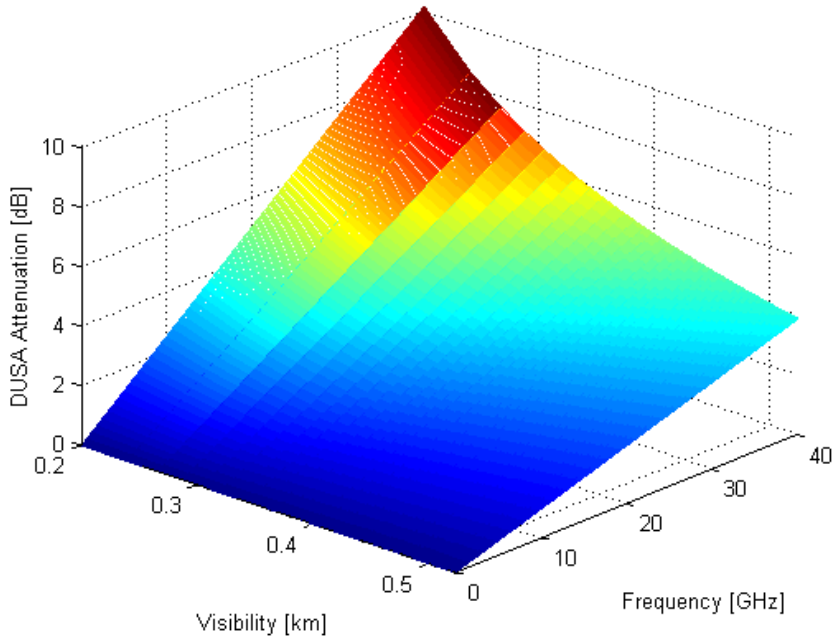

Figure 4 - Simulation results of the total DUSA attenuation on earth-satellite link [27].

In the simulation, a range of visibilities, frequencies and several particles sizes were considered in computing respective attenuations as shown in Figure 4. The dust storm modeling parameters used comprised of a storm with a height of 5 Km in the Eastern region of Saudi Arabia mainly composed of a turbulent clay and silt mixture having a moisture content of 4% [27].

3.4 Example - Effective Downlink Budget for a NIUSAT Link

3.4.1 NIUSAT Introduction

NIUSAT is a Nano satellite designed and developed by Noorul-Islam Center for Higher Education under Noorul-Islam University in India. It has a miniature wide field sensor (MWiFS) for agriculture and disaster management support applications. The satellite images captured through color discrimination will be used for determining agricultural diseases in the crops and plantations. It is also going to provide a much needed timely assistance for disaster management support systems. Another interesting future application include detecting fish rich regions in the oceans.

NIUSAT is planned to be operational in the near future. It will be at the polar sun synchronous orbit operating at LEO altitudes of 560-880 Km at an orbital angle inclination of 97-99. Its orbital period is expected to be 96-100 min. An estimated 225,000 *sq.Km* will be covered by the NanoSAT.

Being a miniaturized satellite with a dry mass (vehicle plus contents, less propellant) of less than 10Kg, the payload is designed to be as minimal as possible. The small solar panels powering the electrical components for example are under tight operation goals to ensure flawless operations. The power limitations onboard the nanoSAT therefore makes the downlink budget a huge concern. All possible meteorological degraders have to be considered in its design. The dust attenuation parameter is considered to this particular nanoSAT downlink budget for the first time. It will be operational at 2.24 GHz (S-Band) for its initial designated mission. However small the initial operation frequency is, the weather degraders have to be considered still, as their effect will be more pronounced due

to the limitations of power aboard the nanoSAT. The maximum values of such degraders along with the newly considered dust and sand attenuation value are listed in Table 2.

The nanoSAT is set to embark on other missions in the future which will be operating at even higher frequencies. The link specifications can be inferred from Table 2 which constitute the input parameters to the downlink computations.

3.4.2 Effective Downlink Budget

Step by step procedure of the downlink budget calculation can be found in [28]. Several other losses were considered with their maximum values at *S*-band to ensure an efficacious link margin. For the first time in [27], the DUSA attenuation parameter was introduced in the downlink budget specifications. The value was extracted from the simulations in the previous section of this proposal. A maximum estimated value of 0.6254 dB, is shown in the table below along with all other losses considered in [28].

Considered Losses	**Max. Value (dB)**
Atmospheric Loss	1
Rain Attenuation	0.5
Fog Attenuation	0.03
Snow Attenuation	0.01
Atmospheric Attenuation	0.2
Ionospheric Loss	0.6
Polarization Loss	0.3
Dust & Sand Attenuation	0.6254

Table 2 - Considered Losses (Maximum values) [27]-[28].

Finally the link budget is redesigned with DUSA attenuation considered. The output parameters are shown in the table below:

Output Parameter	**Value (dB)**
Effective Isotropic Radiated Power (EIRP)	1.9897
Ground Station Antenna Gain	27.0880
Free Space Path Loss	158.5398
Total Losses	161.7652
Received Power at Ground Station	-132.7652
Noise Density at Ground Station Receiver	-207.1389
Received Power to Noise Ratio [P_R/N_0]	74.3736
Bit Energy to Noise Ratio [E_b/N_0] (Available) Bit Rate: *1Mbps*	14.3736
Bit Energy to Noise Ratio [E_b/N_0] (Required) Modulation: *QPSK* BER: 10^{-6}	11.2975
Link Margin	3.0761

Table 3 - Summary of downlink budget output parameters [28]-[29].

The link margin is an important parameter in satellite links and represents the difference between the available and the required value of the bit energy-to-noise ratio. It can be viewed as the amount by which the received power exceeds the receiver sensitivity. In a perfect telecommunication channel this difference should not be there (i.e. zero).

According to the recommendations of the ITU-R (Rec. UIT-R F.1247-1), practical satellite-earth links must maintain a healthy link margin between 2 - 4 *dB* in order to have effective communication links with acceptable QoS. As can be inferred from the output parameters, the NIUSAT's link margin is found to be 3.0761 *dB* which is sufficiently healthy and cost effective for a reliable satellite communication link.

Figure 5 - Link Margin ITU-R (Rec. UIT-R F.1247-1) [28].

4. Basic Formulation: Horizontal Expanse of the Dust Storm

4.1 Modeling of The DUSA Storms & Their Impact on Terrestrial Links

This section is an extension of recent work done by K. Harb, S. Abdillah, and S. Abdul-Jauwad in [27] and briefly covered in the previous section of this proposal. Using the concept of visibility layering, the idea is expanded and applied to the horizontal expanse of the storm. With wind blowing the storm further and further away from its source, the storm will exhibit different levels of visibilities as we move further away from the source where visibility is lowest. In essence the progressing dust plume inherits a three dimensional geometrical structure as shown below:

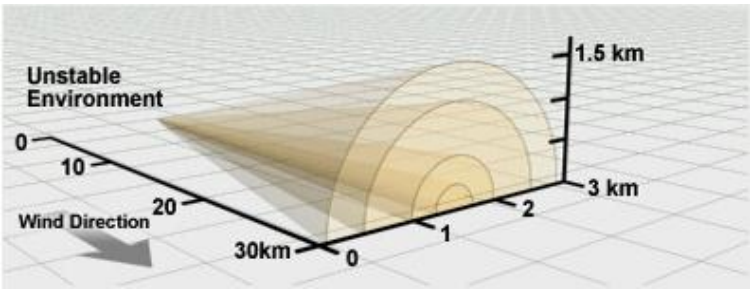

Figure 6 - Three dimensional geometrical structure of a progressing dust plume [7].

As can be deduced from the 3D model, the visibilities will not be a constant value in the storm as dust concentration is non uniform. It will take different values at different points depending on distance from the epicenter and other factors such as wind speed and direction.

The focus of this work will be on the horizontal expanse only where visibility layering is introduced. The variation of visibilities will be modeled along any point to point path link within the storm. Various points along the path link will exhibit different visibilities

hence increasing visibility values away from the storm's epicenter create distinct segments along the terrestrial path that have approximately same average visibility within each of them creating the horizontal layers proposed. This is one of the main research questions. Do these virtual layers actually exist?. It is the objective of this work to also investigate this further through an experiment that is presented in section 5. The question shall be discussed later in the experimental results section 6.6.C.

On a larger picture, the distribution of visibilities will initially be approximated to take an exponential form with visibility values increasing exponentially away from the epicenter. Accurate determination of the distribution of visibilities need thorough experimental work. Also a dummy terrestrial network application scenario will be shown in the same section to further illustrate the importance of this study.

4.2 Visibility Layers on the Horizontal Expanse & Attenuation

The characteristic visibility exhibited in dust plumes is approximated to be an exponential function given by:

$$V = V_0 * exp\left(\frac{x}{x_r}\right) \qquad \textbf{(12)}$$

where x is the distance from the epicenter of the plume, V_0 is the minimum visibility at the storm epicenter and x_r is the characteristic radial distance over which the minimum visibility will increase by a factor of $exp(1)$. Simultaneous equations can be formed using measured values of visibility V and their corresponding distance x of occurrence to approximate the constants V_0 and x_r. For simulation purposes, the constants shall be

adopted from the observed dust storm in [23] which were estimated to be V_0 = 1.84×10^{-3} Km and x_r = 9.26 Km.

Figure 7 shows the simplified model of a progressing dust storm. It is of interest therefore to estimate visibility value at any given distance x_i away from the epicenter. Thus rewriting equation (12) we have:

$$V(x_i) = V_0 * \exp\left(\frac{x_i - x_0}{x_r - x_0}\right) \qquad \textbf{(13)}$$

where $x_i > x_0$ and x_0 is the radial distance for the region (epicenter) over which the visibility is lowest (V_0). This generic model of visibility can apply to any typical storm as the focus of determining the storm's impact on a radio link in terms of attenuation is on a straight (point-to-point) path within the storm's path. The conditions on the ground will dictate the direction of the distances (x_i). It is also important to note that to determine any $V(x_i)$, the storm's exponential shape has to be temporarily frozen in space.

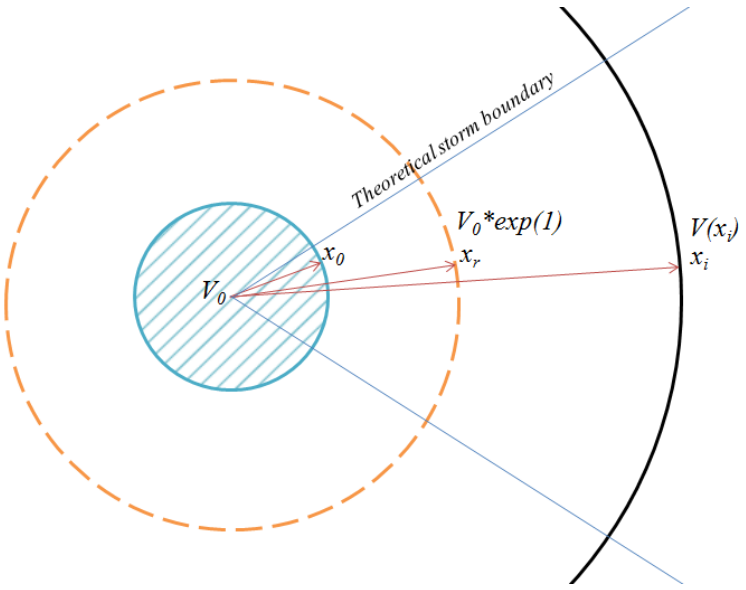

Figure 7 - Simplified model of a progressing dust storm (top view).

Equation (13) can now be used to predict attenuation along a given terrestrial path link under conditions of dust. Zain and his team [25] in Sudan introduced a prediction equation that estimated attenuation given a certain frequency of operation and visibility. Using equation (13) on their attenuation model, we can recursively calculate the attenuation depending on visibility values at a particular location. The novel idea of visibility layering brings more accuracy and flexibility to their model as shown below:

$$A'_{P_i} = \frac{R_{eq} f}{V(x_i)} \left(K + W(R_{eq} f)^2 + S(R_{eq} f)^3\right) \qquad [dB/Km] \tag{14}$$

where A'_{P_i} is the point attenuation in *dB/Km*, R_{eq} is the equivalent particle radius in meters of the particles forming the dust storm, f is the operational frequency of the link in *GHz*, and *K*, *W* and *S* are constants that are dependent on the real and imaginary parts of the particle's permittivity values as defined in [25]:

$$K = \frac{1886 * \varepsilon''}{(\varepsilon' + 2)^2 + \varepsilon''^2} \tag{15}$$

$$W = 1.37 \times 10^5 * \varepsilon'' \left\{ \frac{6}{5} \frac{7\varepsilon'^2 + 7\varepsilon''^2 + 4\varepsilon' - 20}{[(\varepsilon' + 2)^2 + \varepsilon''^2]^2} + \frac{1}{15} + \frac{5}{3[(2\varepsilon' + 3)^2 + 4\varepsilon''^2]} \right\} \tag{16}$$

$$S = 3.79 \times 10^6 \left\{ \frac{(\varepsilon' - 1)^2(\varepsilon' + 2) + [2(\varepsilon' - 1)^2(\varepsilon' + 2) - 9] + \varepsilon''^4}{[(\varepsilon' + 2)^2 + \varepsilon''^2]^2} \right\} \tag{17}$$

In presence of humidity like in most regions closer to the sea or large water bodies, the real and imaginary parts of the permittivities will be adjusted according to the relative humidity (H%) present in the atmosphere as done in [32] and [28].

$$\varepsilon'_H = \varepsilon' + 0.04H - 7.78 \times 10^{-4}H^2 + 5.56 \times 10^{-6}H^3 \quad \textbf{(18)}$$

$$\varepsilon''_H = \varepsilon'' + 0.02H - 3.71 \times 10^{-4}H^2 + 2.76 \times 10^{-6}H^3 \quad \textbf{(19)}$$

The point attenuation is finally modified and presented by multiplying equation (14) with a unit-less volume summation of all probabilities of particles sizes occurring in each of the layers multiplied by the cubic of their normalized particle radii, r'_i as follows:

$$A_{P_i} = \frac{R_{eq}f}{V(x_i)}\left[K + W(R_{eq}f)^2 + S(R_{eq}f)^3\right]\sum_i P_i r'^3_i \quad dB/Km \quad \textbf{(20)}$$

These point attenuations can now be summed up over the entire path length traversed by the microwave signal to get the total dust and sand attenuation.

4.3 Simulations Results

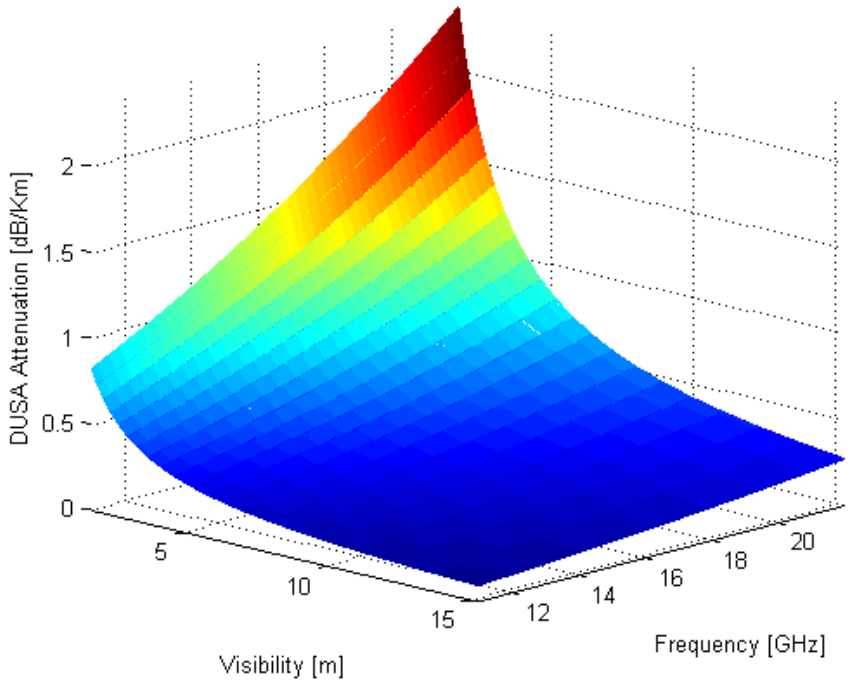

Figure 8 - Output of the attenuation simulation.

In the simulation, a range of visibilities, frequencies and several particles sizes were considered in computing respective point attenuations as shown above. The dust storm modeling parameters used comprised of a storm in the Eastern region of Saudi Arabia mainly composed of a turbulent clay and silt mixture having a moisture content of 4%.

The results indicate that at very intense dust storms, microwave links will be seriously degraded. Extreme rare cases can lead to total link unavailability. Attenuation values beyond 2.5 dB/Km can be realized at KU and KA bands operation.

The exponential variation of visibility from the epicenter has a consequence to the amount of attenuation caused at each region when the storm is propagating and thus the model can be used to predict how bad a dust storm could impact a terrestrial link

operating at some given frequency band. This is a more accurate and efficient computation of the degradation of radio links under dusty conditions. The flexibility of the model enables variation of the input variables for any given ground conditions.

As part of future expansion of this model, the effect of angle on the radial variation of visibilities from the storm's epicenter shall be investigated.

5. DUSA Outage and Planning

Dust and sand storms is one of the major meteorological problems that microwave communications experience in the arid and semi arid regions across the globe. Since their occurrence is of random nature, the effects due to them is different in different regions of the world.

Various arid and semi arid regions have unique properties in respect to their soil textural class inherent in them. In addition factors like humidity and wind speeds prevalent in such dust prone regions, will contribute largely in the dynamic structure of the storm and composition of the airborne sand and dust particles. This has a direct impact on the visibilities to be experienced during the dust storm events, which determines the severity of the storms.

Just like other meteorological degraders such as rain, it is similarly important to plan for DUSA outages in microwave system design. Using existing DUSA storm parameters from studies done in literature and the generic models found in earlier sections, a microwave system designer can depend with reasonable reliability on the geo-specific data in the coverage area to estimate the DUSA outage they need to budget for in advance in order to achieve acceptable QoS meeting the desired system operation levels.

Table 4 for example, shows a summary of the world's largest deserts and their most abundant soil types as can be seen from Figure 9 and Figure 10 respectively.

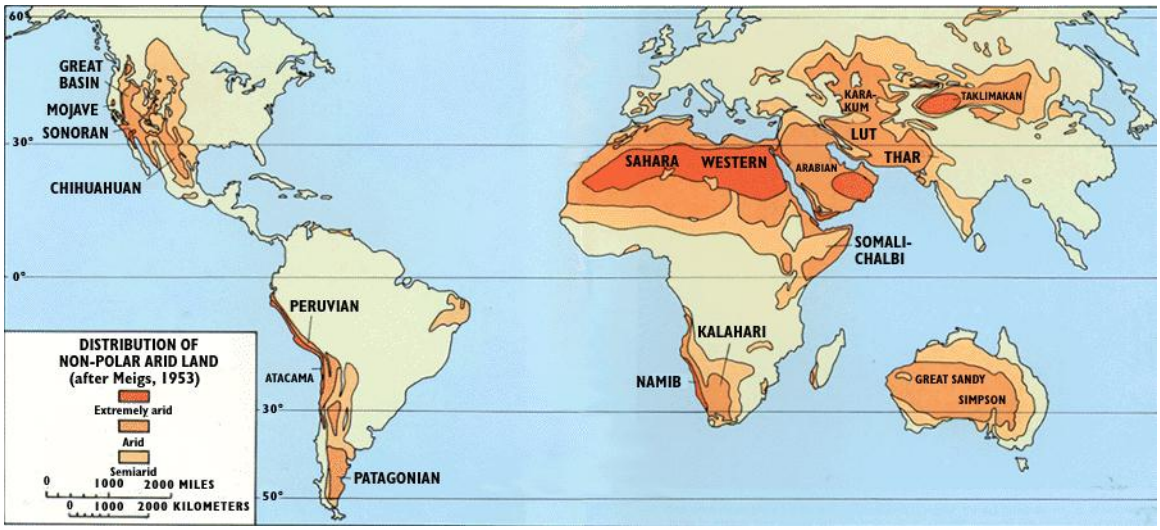

Figure 9 - A world map showing the largest arid and semi-arid regions on the globe.

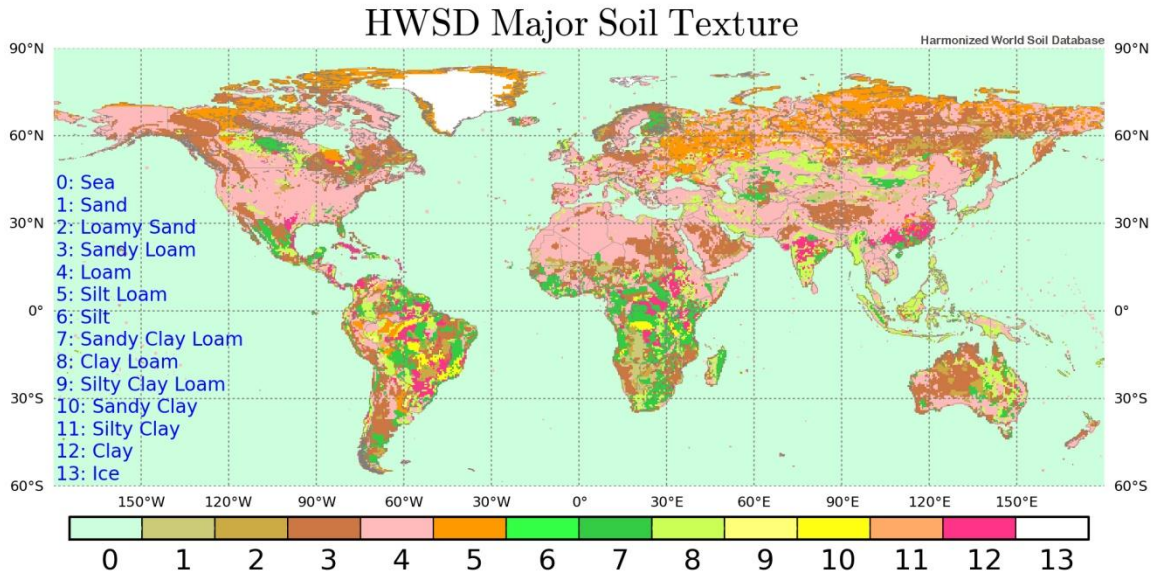

Figure 10 - The harmonized world soil database (HWSD) major soil texture classes of the world's soils.

REGION	DESERT NAME	SOIL TYPE	PERMITTIVITIES	MOISTURE CONTENT (%)	FREQ. BAND (GHz)
MIDDLE EAST	ARABIAN DESERT	Sandy	4.4-j0.2024	4	S - (1-4)
		Sandy	3.6-j0.432	4	X - (8-12)
		Sandy	3.9-j0.62	5	KU - (12-18)
		Silty Clay	3.4-j0.2	3	K - (18-26.5)
		Sandy	3.6-j0.65	5	KA - (26.5-37)
AFRICA	SAHARA DESERT	Clay	2.20-j0.034	0	S - (1-4)
	SUMALL DESERT	Loamy	2.44-j0.003	0	X - (8-12)
	KALAHARI DESERT	Silty Clay	4.7-j1.1	12	K - (18-26.5)
	NAMIB DESERT	Sandy Loamy	2.45-j0.375	5	KA - (26.5-37)
ASIA	TURKESTAN DESERT	Loamy	13.8-j2.484	13	X - (8-12)
	THAR DESERT	Fine Sand	5.5-j1.3	10	KU - (12-18)
	GOBI DESERT	Sandy Clay	3.290-j0.728	10	KA - (26.5-37)
AUSTRALIA	AUSTRALIAN DESERT	Sandy Loam	2.53-j0.01	0	X - (8-12)
		Sandy Loam	2.8-j0.035	0.3	KU - (12-18)
		Sandy Loam	2.515-j0.073	0	KA - (26.5-37)
SOUTH AMERICA	SECHURA DESERT	Sandy	3.9-j0.62	5	KU - (12-18)
	ATACAMA DESERT	Loamy	4-j1.325	10	KA - (26.5-37)
NORTH AMERICA	SONORAN DESERT	Sandy	5.5-j1.3	10	KU - (12-18)
	MOJAVE DESERT	Loamy	2.53-j0.065	0	KA - (26.5-37)

Table 4 - Summary of the major world desert regions, their soil textural and dielectric properties. Different permittivities are adopted from Table 1 as published in literature.

In this work, the regions of Middle East and North Africa shall be the main focus. This is due to the unavailability of dust storms data and patterns in the other arid regions. The two regions are the major contributors of global dust storms in the world. Model simulations for example show that the Middle East alone contributes to 20% of the global total dust emissions [29].

5.1 Dust Storm Data Source

The Barcelona Dust Forecast Center (BDFC) [30] is a rich source of dust storm data operated by the World Meteorological Organization (WMO) and has huge databases of dust storm related information for the regions of Middle East and North Africa. The

center is a specialized meteorological center with activity specialization on atmospheric sand and dust forecast (ASDF).

It is important to point out that the center provides forecast data only and not real actual data. In this work only 1 year data (Feb 2014 - Feb 2015) is used for the analysis in the sub-sections to follow.

One of the parameters of interest that the center records and tracks is the dust surface concentration. It represents the concentration of dust by mass per unit cubic volume near the surface of the earth. This measure is thus valid for dust attenuation analysis for terrestrial microwave link communications as it gives surface dust data and not dust data high in the air (needed for attenuation analysis for satellite communications).

Therefore the dust outage planning in this section will only focus on the terrestrial links. Other parameters available at the BDFC archives could be useful to explicate a similar analysis for the case of satellite links DUSA outage planning.

5.2 Analysis of Dust Surface Concentration Data

Having the dust surface concentration data over time, one can further classify by subdividing the two major regions based on the dust concentration levels recorded and the frequency at which they occur into distinct zones. To plan for dust outage, a system designer can then focus on specific zones in which his system will be covering and operating.

The BDFC archives presents the forecasted surface concentration data in a 3 hourly period during each day. The entire year data is downloaded as archived by queuing the individual links using a standard download manager.

A sample dust forecast image downloaded from the archives is shown below:

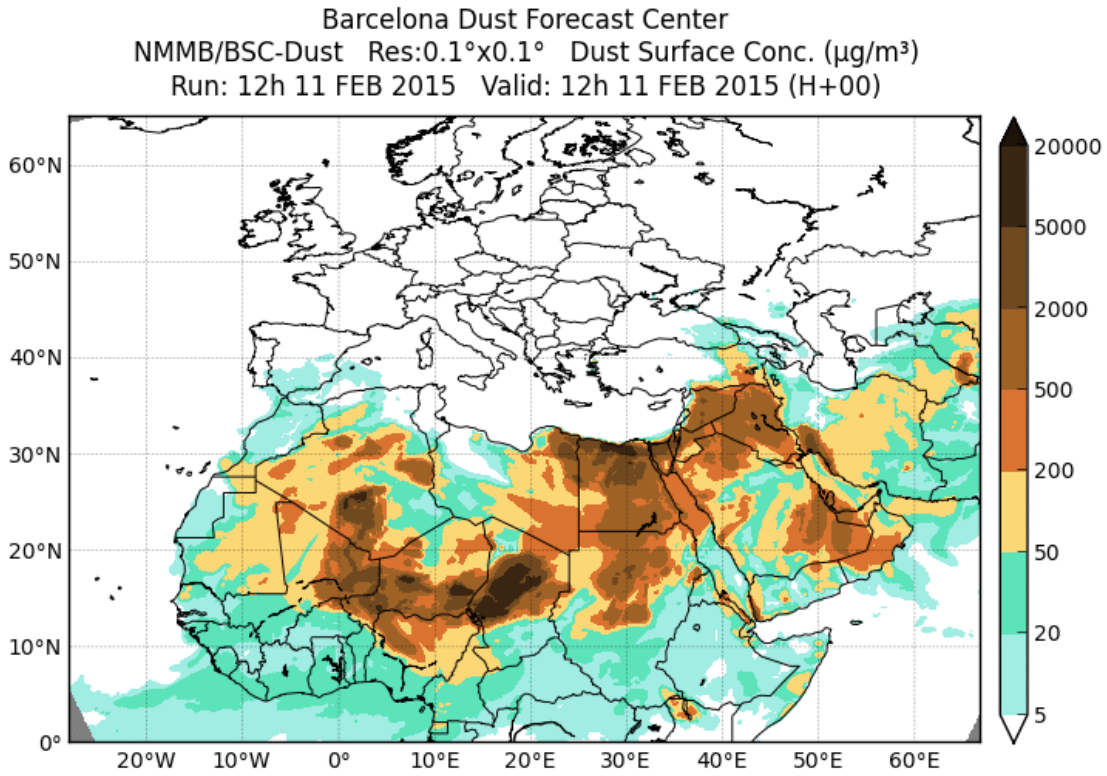

Figure 11 - Sample dust surface concentration forecasted on 11 Feb 2015.

The figure basically gives the dust surface concentration levels (given in a range) as forecasted at that day and time.

As part of an extensive analysis, the entire 1 year archive of the raw graphic data is imported in Matlab for processing. Each image is scanned for pixel data to cumulatively map the number of times (frequency) a given concentration level was forecasted after every 3 hours for the whole year (annual). With the resultant matrix, the contour function is then used to plot the 8 concentration ranges. The results are then superimposed over a

clear high resolution map to give a more meaningful picture (giving an idea of location) of the frequency of the forecasted concentration ranges at each point on the studied region (0 South, 65 North, -28 West, 67 East).

The 8 results are shown below starting from the lowest dust surface concentration range of 5-20 $\mu g/m^3$ to the highest range of beyond >20000 $\mu g/m^3$:

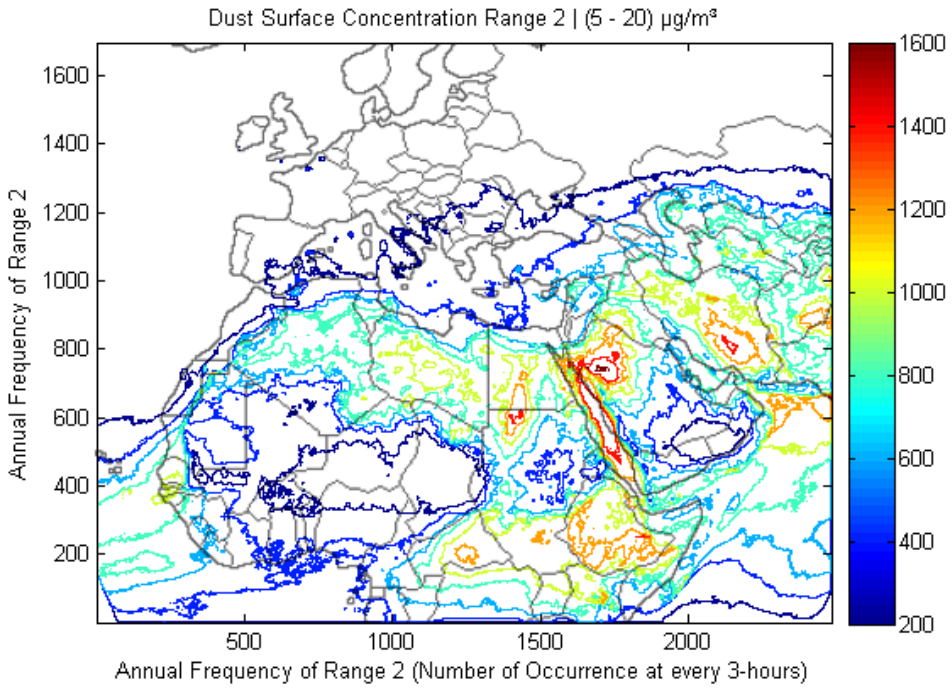

Figure 12 - Occurrence of dust surface concentration range 2 (5-20 $\mu g/m^3$) every 3 hours.

To give an idea of the meaning of the color-bar to the right of each of the results, the values of the color-bar in figure 12 above are used. The numbers on the colored scale represent the frequency (defined here as number of times) that the particular dust surface concentration level was forecasted (in this specific example, range 2 of 5-20 $\mu g/m^3$) at 3-hourly period for the whole year. Since there are eight 3-hour periods in a day, dividing 1600/8 gives 200 days which is the duration in days that range 2 concentration was forecasted in the regions traced with that particular color.

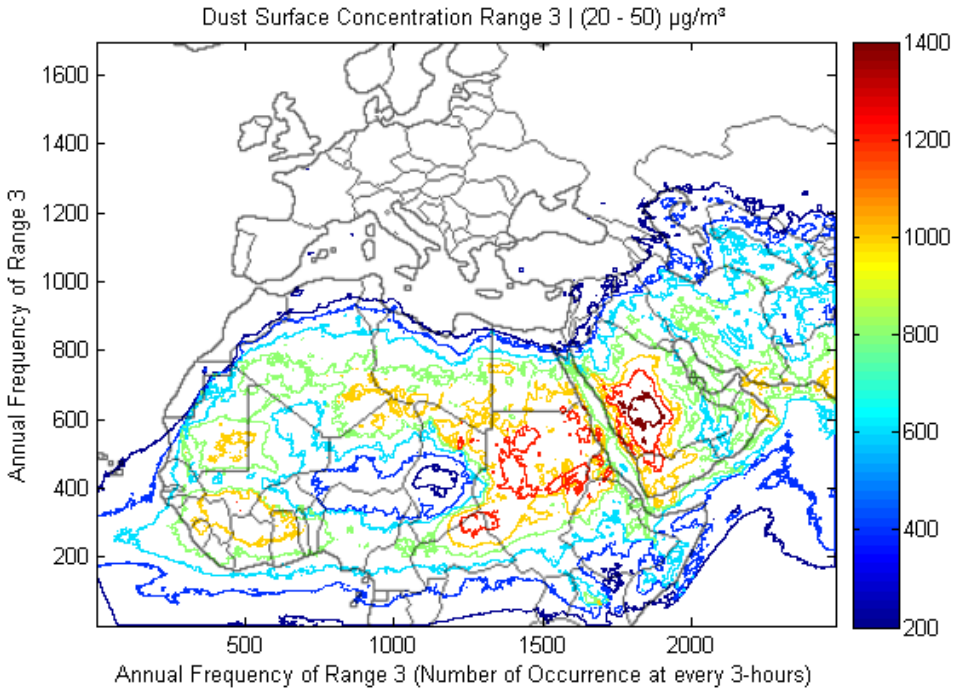

Figure 13 - Occurrence of dust surface concentration range 3 (20-50 *µg/m³*) every 3 hours.

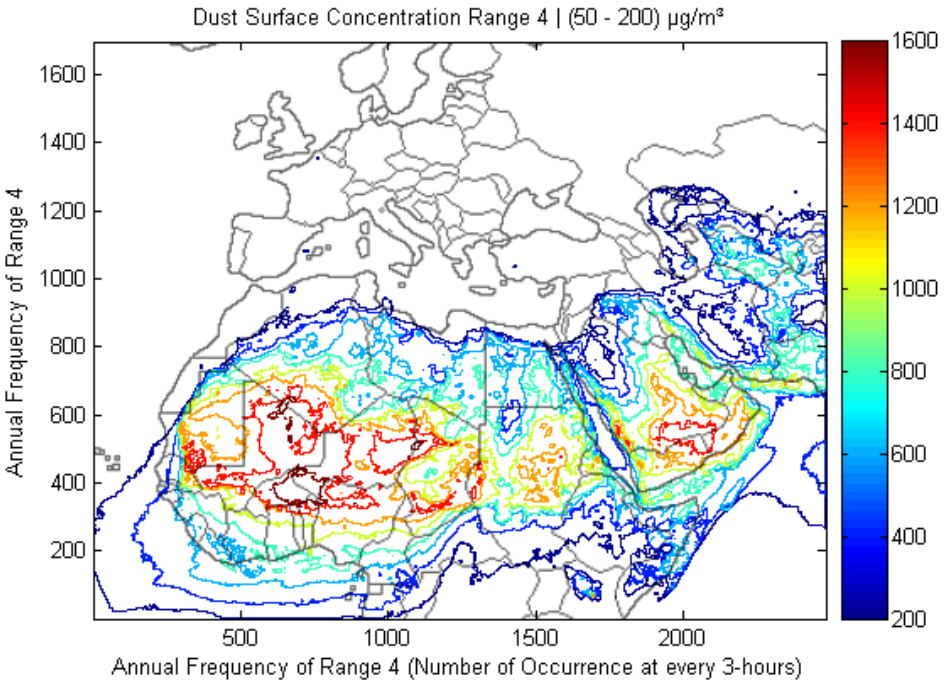

Figure 14 - Occurrence of dust surface concentration range 4 (50-200 *µg/m³*) every 3 hours.

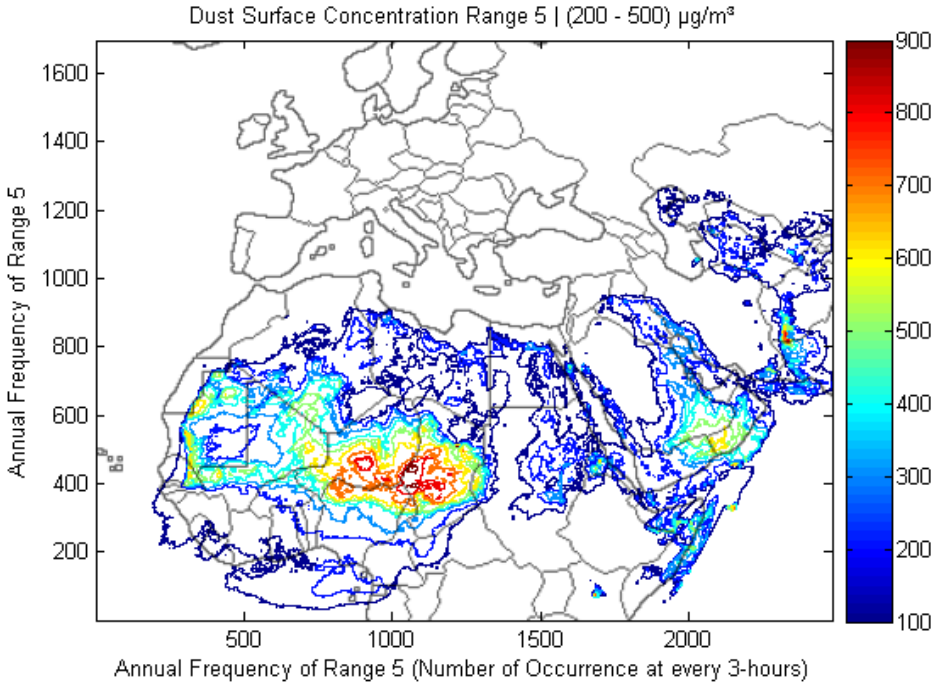

Figure 15 - Occurrence of dust surface concentration range 5 (200-500 *µg/m³*) every 3 hours.

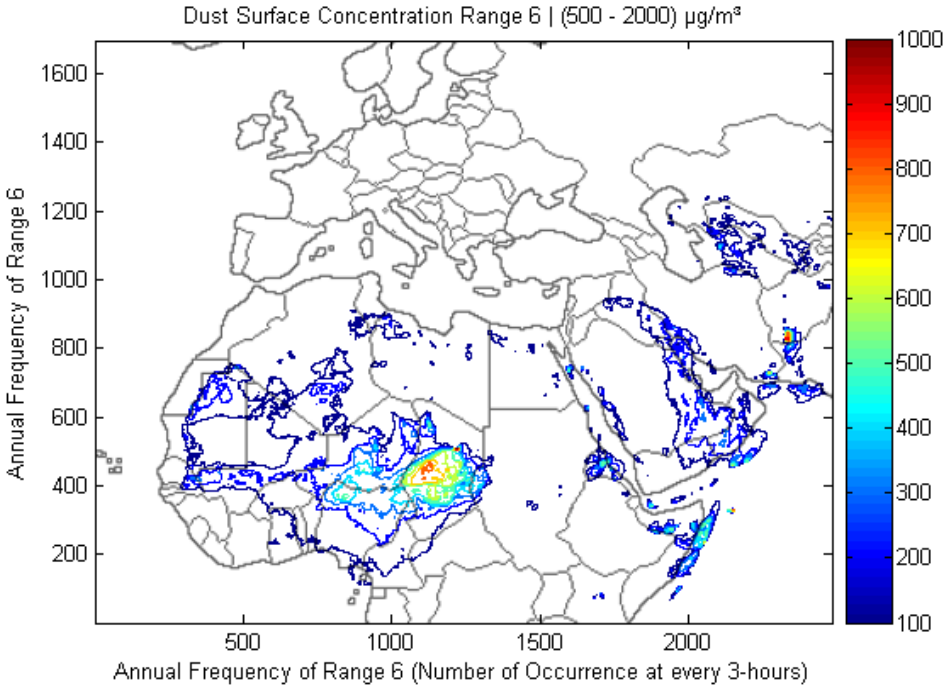

Figure 16 - Occurrence of dust surface concentration range 6 (500-2000 µg/m³) every 3 hours.

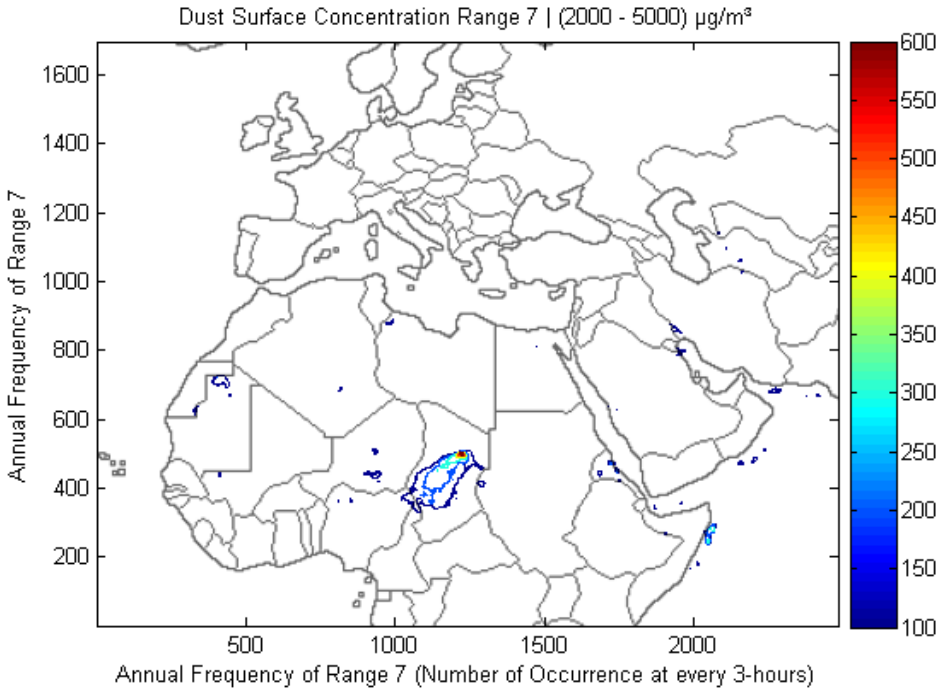

Figure 17 - Occurrence of dust surface concentration range 7 (2000-5000 µg/m³) every 3 hours.

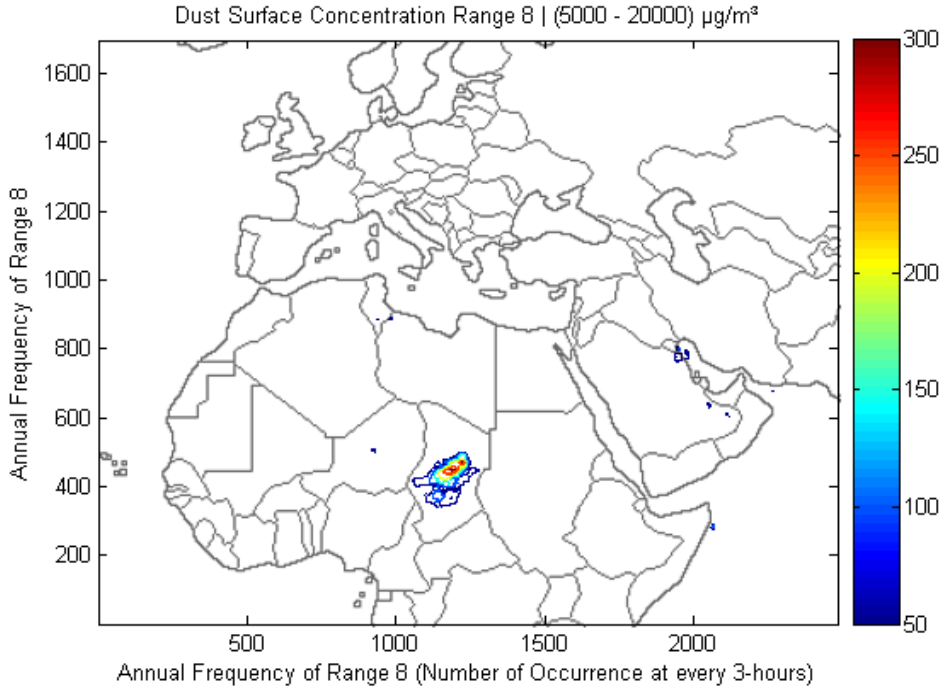

Figure 18 - Occurrence of dust surface concentration range 8 (5000-20000 µg/m³) every 3 hours.

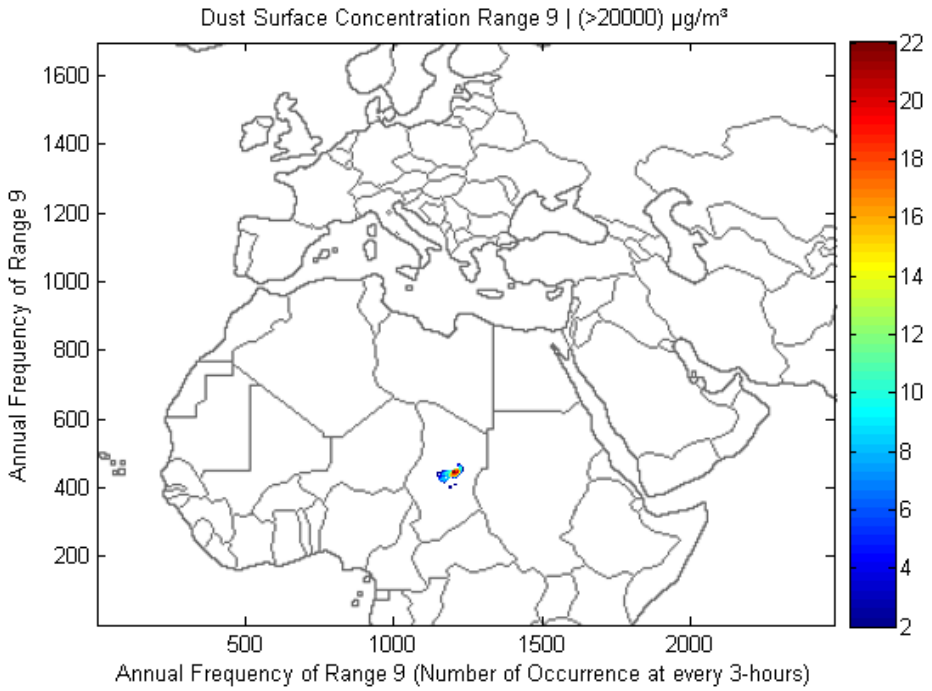

Figure 19 - Occurrence of dust surface concentration range 9 (>20000 µg/m³) every 3 hours.

5.3 Dust Surface Concentration to Visibility Translation

The dust surface concentration data is then translated to visibility which is our major variable of concern. The severity and classifications of the storms will be dependent on the visibilities exhibited during the dust storm events. Severe dust storms will have much reduced visibility (increasing dust effects) and light storms will have improved visibility levels.

Yaping Shao in [31] provided an empirical relationship derived by fitting dust surface concentration measurements to visibility. For a given dust concentration, visibility can be estimated from their relation as follows:

$$C = \begin{cases} 3802.29V^{-0.84} & V < 3.5 \\ exp(-0.11V + 7.62) & V \geq 3.5 \end{cases} \quad \textbf{(21)}$$

where V is the visibility in [*Km*] and C is the dust surface concentration in [$\mu g/m^3$]. The first part (for V<3.5 *Km*) of the relation is the one relevant to this study with respect to the visibilities exhibited during dust storms.

5.4 General Dust Storm Zones for Middle East & North Africa

Processing of the one year (Feb 2014 - Feb 2015) archived data from the BDFC leads to the following general dust storm zones shown in Figure 20. This was done by summing up the products of the cumulative frequency of occurrence of individual surface dust concentration levels and the actual upper limit of each range (i.e. 5, 20, 50, 200, 500, 2000, 5000 and 20000 $\mu g/m^3$). A standard photo editor then was used to clearly draw the zones as labeled below:

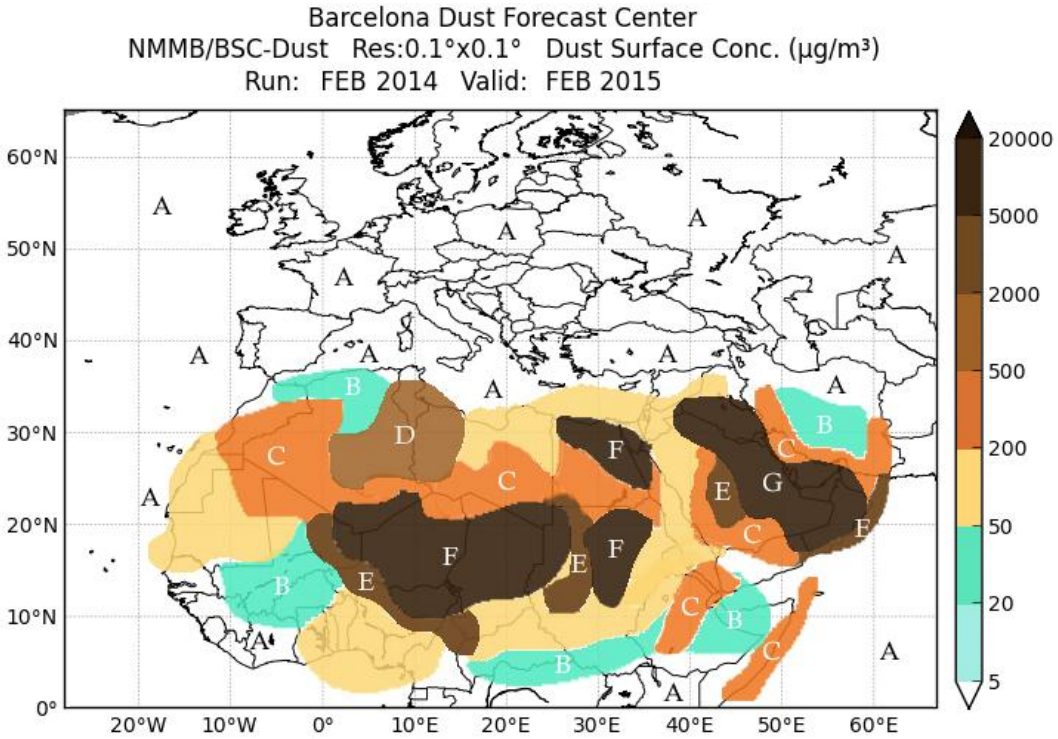

Figure 20 - Major dust storm zones of the North Africa and Middle East.

Dust Surf. Conc. [µg/m³]	<20	20-50	50-200	200-500	500-2000	2000-5000	5000-20000
Visibilities [Km]	-	-	-	11.2 - 33.3	2.1 - 11.2	0.7 - 2.1	0.1 - 0.7
Dust Zone	Number of Days Out of 365						
A	332	17	6	7	3	0	0
B	94	236	21	12	1	1	0
C	25	21	101	145	38	26	9
D	17	66	143	106	19	12	2
E	103	91	79	64	18	7	3
F	20	30	36	57	77	97	48
G	107	65	59	44	36	30	24

Dust Surf. Conc. [µg/m³]	<20	20-50	50-200	200-500	500-2000	2000-5000	5000-20000
Visibilities [Km]	-	-	-	11.2 - 33.3	2.1 - 11.2	0.7 - 2.1	0.1- 0.7
Dust Zone	Annual Occurrence in Percentage						
A	90.96%	4.66%	1.64%	1.92%	0.82%	0.00%	0.00%
B	25.75%	64.66%	5.75%	3.29%	0.27%	0.27%	0.00%
C	6.85%	5.75%	27.67%	39.73%	10.41%	7.12%	2.47%
D	4.66%	18.08%	39.18%	29.04%	5.21%	3.29%	0.55%
E	28.22%	24.93%	21.64%	17.53%	4.93%	1.92%	0.82%
F	5.48%	8.22%	9.86%	15.62%	21.10%	26.58%	13.15%
G	29.32%	17.81%	16.16%	12.05%	9.86%	8.22%	6.58%

Table 5 - Approximate overview of the number of days certain visibilities were experienced during the period Feb 2014 - Feb 2015 in the major dust storm zones. Equivalent visibilities translated from equation (21).

Dust surface concentration levels beyond 2000 $\mu g/m^3$ are of interest in respect to the effects they will have on microwave communication. Translating to visibility levels of 2.1 *Km* and below.

The data from the BDFC meteorological center archives maps the data on scale with a highest value of 20000 $\mu g/m^3$ and beyond which translates to a visibility of 0.1 *Km* and further below.

The relationship between the dust surface concentration and visibility is further illustrated by plotting first part (for $V<3.5$ *Km*) of equation (21) below:

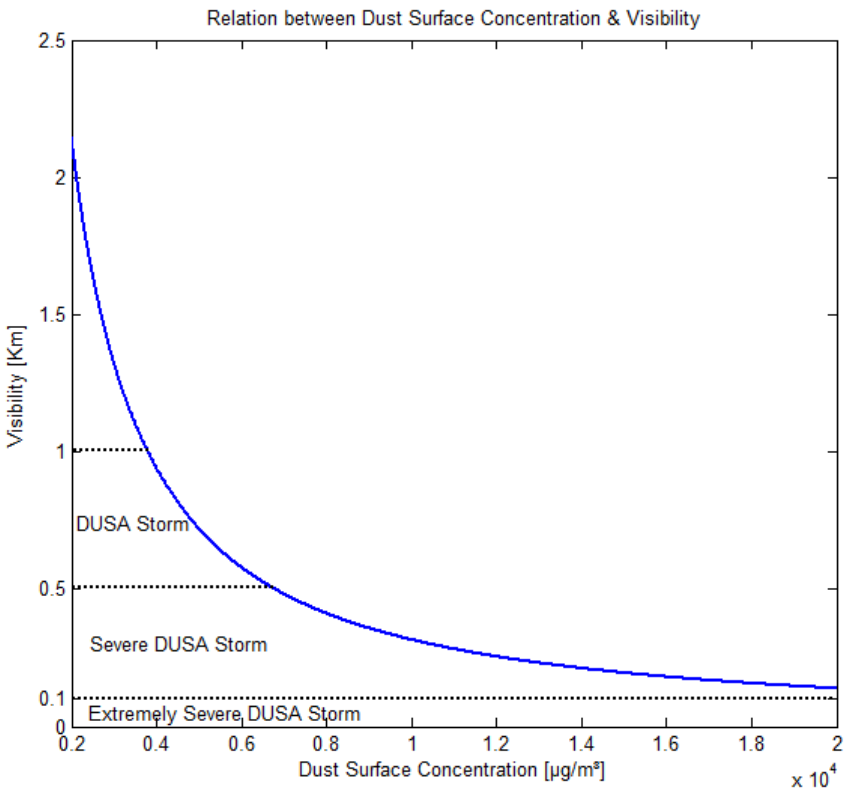

Figure 21 - Translation of dust surface concentration to visibility.

5.5 DUSA Outage Planning for Terrestrial Communications

To be classified as a dust storm, the visibility must be smaller than 1 *Km*. When the visibility is shorter than 500 *m*, it is called a "severe dust storm" [23]. Thus the system designer can only focus on the last two columns of Table 5 (highlighted by non-green) and the visibility regions below 1 *Km* as indicated above.

The system designer planning for the dust storm events will have to choose the region in which the microwave system will be covering (from Figure 20), the soil textural class common in that region (from Figure 10), the operational frequency to be used from Table 4. The designer also will use the zones and their corresponding dust surface

concentration levels (from Table 5) to decide on what levels of severity (visibilities) he wishes to plan for as shown in Figure 21.

The designer will then use any of the following figures that matches the ground parameters for his terrestrial microwave system coverage area to determine the corresponding attenuation due to DUSA storm that he will include in his link budget design.

Soil-Type: Loamy
[Africa | South America | North America | Asia]

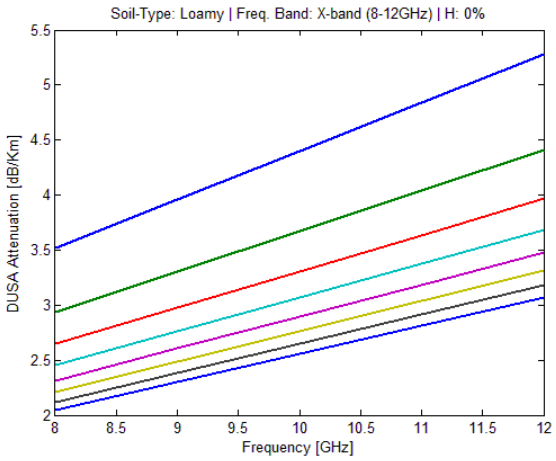

Figure 22 - DUSA Outage with Soil-Type: Loamy, Freq. band: X-band (8-12GHz), Humidity content: 0%

Soil-Type: Loamy
[Africa | South America | North America | Asia]

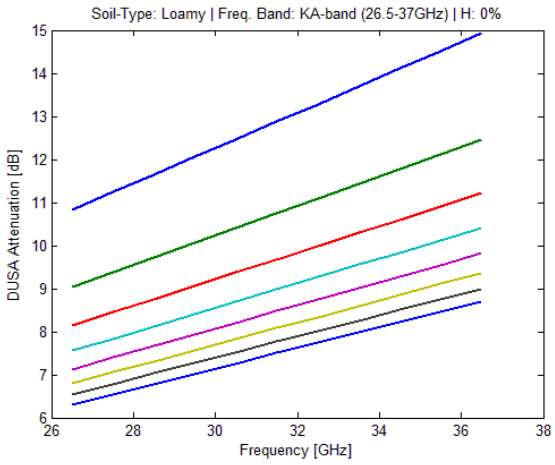

Figure 23 - DUSA Outage with Soil-Type: Loamy, Freq. band: KA-band (26.5-37GHz), Humidity content: 0%

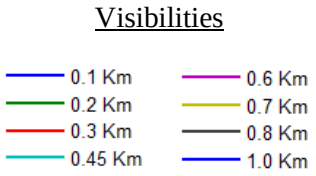

Soil-Type: Sandy-Loam
[Australia | Asia]

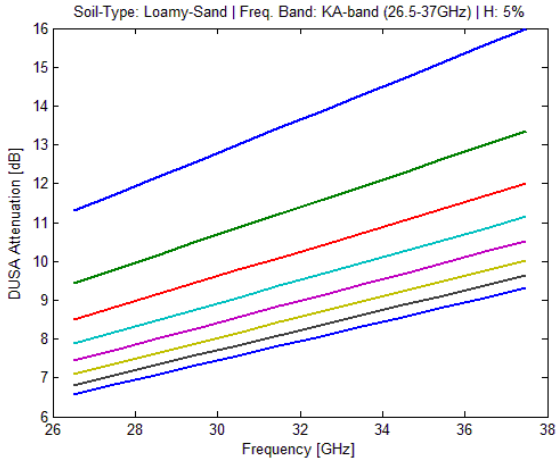

Figure 24 - DUSA Outage with Soil-Type: Sandy-Loam, Freq. band: KA-band (26.5-37GHz), Humidity content: 5%

Soil-Type: Sandy
[Middle East | South America | North America]

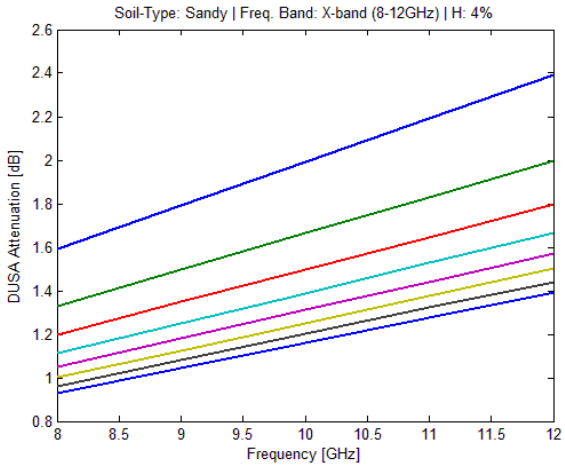

Figure 26 - DUSA Outage with Soil-Type: Sandy, Freq. band: X-band (8-12GHz), Humidity content: 4%

Soil-Type: Silty-Clay
[Middle East | Africa | Asia]

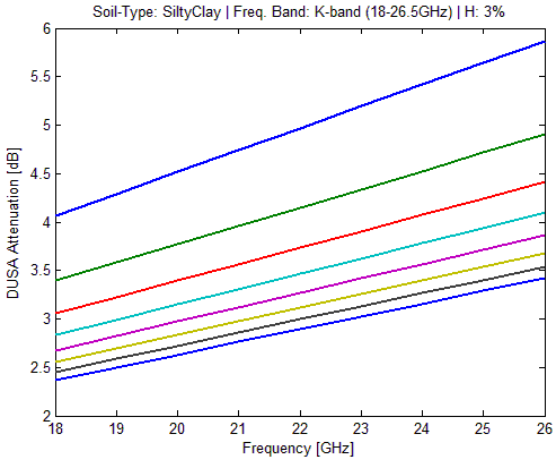

Figure 25 - DUSA Outage with Soil-Type: SiltyClay, Freq. band: K-band (18-26.5GHz), Humidity content: 3%

Soil-Type: Sandy
[Middle East | South America | North America]

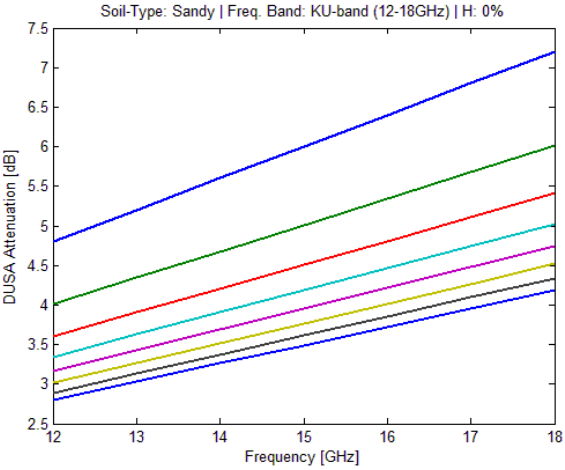

Figure 27 - DUSA Outage with Soil-Type: Sandy, Freq. band: KU-band (12-18GHz), Humidity content: 0%

Visibilities

Soil-Type: Sandy
[Middle East | South America | North America]

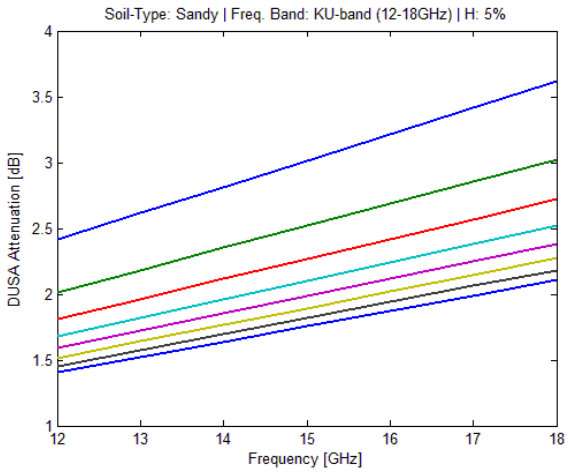

Figure 28 - DUSA Outage with Soil-Type: Sandy, Freq. band: KU-band (12-18GHz), Humidity content: 5%

Soil-Type: Sandy
[Middle East | South America | North America]

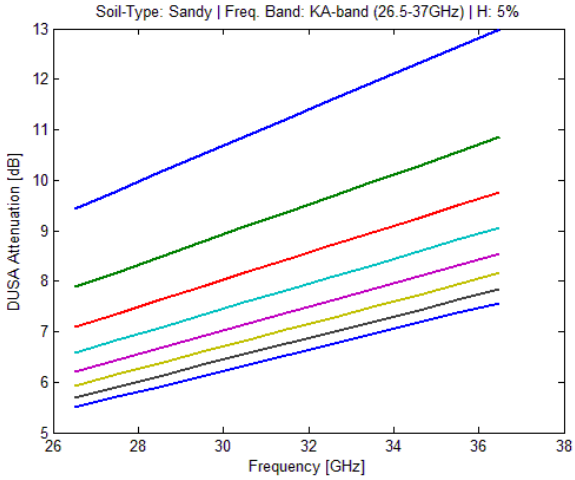

Figure 29 - DUSA Outage with Soil-Type: Sandy, Freq. band: KA-band (26.5-37GHz), Humidity content: 5%

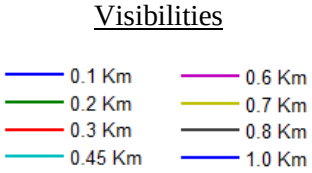

As can be deduced from the above figures, the dust storm effects become serious at higher frequency operation and severe dust storm visibilities.

Once the designer extracts the attenuation level from the most appropriate figure for his ground conditions and system operation specifications, the information is then used in the link budget computations.

This will enable setting early plans to pre-mitigate the severe effects caused by DUSA storms on terrestrial microwave communications.

6. Experimental Work

6.1 Motivation for Experiment

Since dust storms are a complex phenomenon, it is critical to try out some experiments in order to shed more light on their behavior and physical structure. Understanding this will enable engineers to come up with more effective solutions and means to mitigate the potential attenuations due to dust and sand storms.

The figure below shows a typical dust plume overall visibility distribution as the storm grows and expands from its epicenter. As postulated before, regions far away will have less particles concentration hence improved visibility.

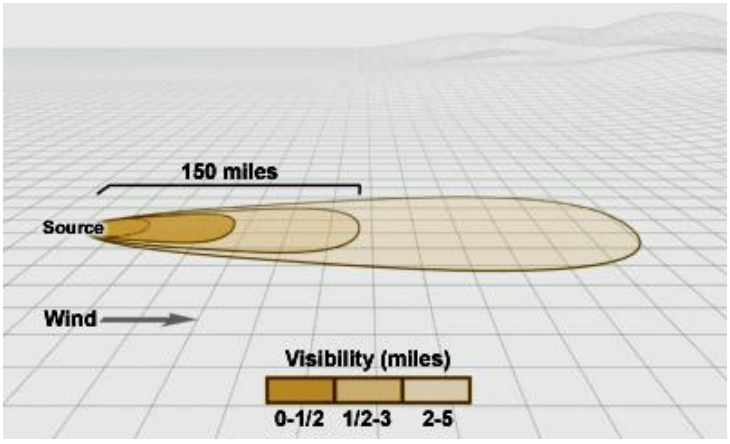

Figure 30 - Variation of visibilities on the horizontal expanse [7].

The proposed experiment tries to study the existence of visibility layers on the horizontal side of the storm and show their effect on radio link design and operation during storm events. These varying visibility profiles form the virtual layers proposed in earlier work on the vertical expanse of the storm. If this is understood, we can know how exactly will a microwave signal be affected as it travels along the storm. Each visibility layer will impact the electromagnetic energy in the signal differently hence an intelligent feedback system can be developed to compensate for the suffered degradation according to the

visibility profile of that particular region. This can be further elaborated using the example below:

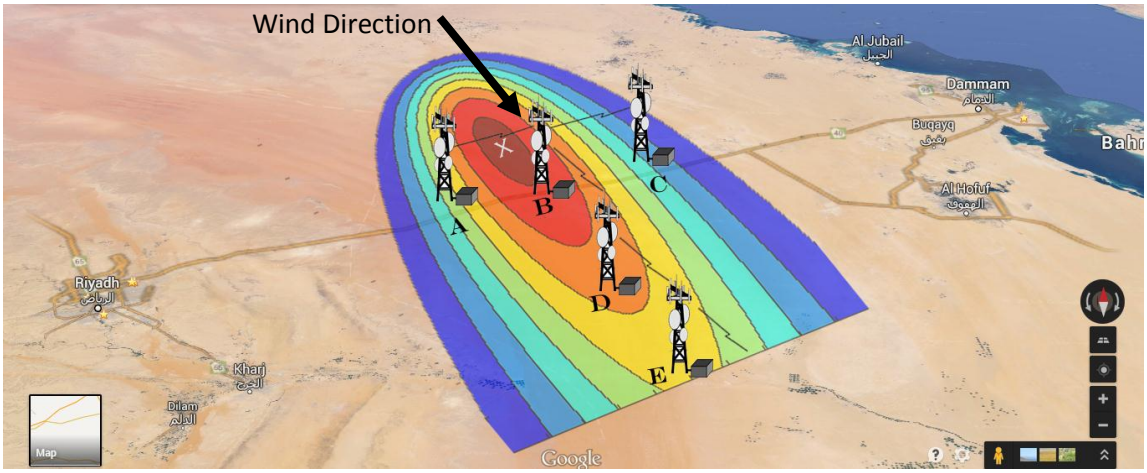

Figure 31 - A dummy terrestrial network vulnerable to DUSA storms.

The figure above is for illustrative purposes and does not represent a schematic of a real communication system. In addition, the region chosen is an example only. This terrestrial microwave point to point base station sub-system is assumed to cover the Riyadh-Dammam highway as well as branching to other cities along the highway, servicing the various mobile stations in the region. The microwave powered sub-system can be thought of as part of a GSM network rolled out by one of the mobile service providers.

Assuming a dust storm system develops from the epicenter at location X and wind blowing southwards, the storm will traverse the highway as shown. As the storm build up and progresses, each base station in the network will experience different levels of dust storm intensities. Regions closer to the epicenter will face the worst part of the dust storm. Communication to nearby base stations could be crippled during the dust storm event thereby affecting service delivery in the region.

If this behavior is well quantified and anticipated then service providers can plan and mitigate the dust storm effects more effectively. For example, each affected base station in the network can thus intelligently adjust its transmitting power or modulation scheme to mitigate the wireless signal attenuation encountered within its region in the highway.

Therefore studying this phenomenon is necessary to design robust and effective network systems for any desired application in areas prone to dust and sand storms like the Middle East.

6.2 Experiment Methodology

A number of methods were considered for use in the experiment and a practical method using an optical telescope was chosen to conduct observations with the aim of studying the structure of the dust storm.

An optical telescope's ability to focus far targets is of great advantage in regards to the experiment. Light sources very far from a reference point can be detected and captured in real time for visibility analysis using their intensity profiles.

The limitations of this methodology has been highlighted at the end of this report in section 6.7.

6.3 Experiment Tools

The experiment is setup as shown in Figure 32 where an ETX-90 MEADE telescope is used to focus on the far light point sources chosen. A web camera mounted at the back of the telescope captures the images for analysis in an advanced image analysis software.

Figure 32 - Experimental setup.

The ETX-90 telescope's main specifications are tabulated below:

Optical Design	Maksutov-Cassegrain
Primary Mirror Diameter	96 mm
Clear Aperture, D	90 mm
Focal Length	1250 mm
Focal Ratio	f/13.8
Input Voltage	12 V (DC)

Table 6 - The ETX-90 telescope specifications

The web camera used had to be a little bit modified to fit into the back of the telescope. The front outer case protecting the components inside were removed to fit in the ETX telescope perfectly. The removal of the protective case exposes the array of the complementary metal oxide semiconductor (CMOS) sensor to the incoming photons.

Without the camera mounted at the back of the telescope, target images cannot be captured for analysis. The pictures below shows the web camera and how it was mounted at the back of the telescope.

Figure 33 - The Microsoft LifeCam Cinema (H5D-00001) web camera model used.

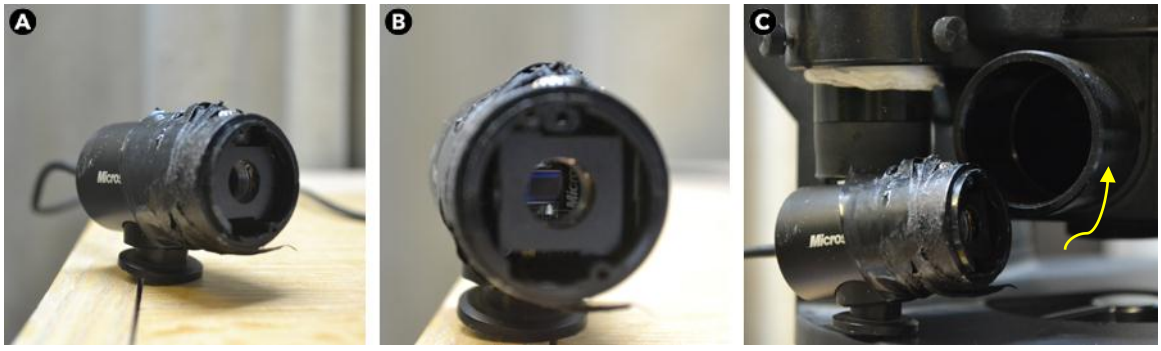

Figure 34 - **(A)** The web camera's protective front seal and stand stripped off. **(B)** Front view of the stripped off camera showing the inside components and the CMOS sensor. **(C)** The modified camera ready to be mounted to the back of the telescope as shown by the arrow.

The specifications of the web camera are tabulated below:

Model Name	Microsoft LifeCam Cinema (H5D-00001)
Sensor Technology	Complementary Metal Oxide Semiconductor (CMOS)
Maximum Resolution	1280 x 720
Video	Up to 30 Frames per Second
Technologies	TrueColor Technology; ClearFrame Technology

Table 7 - The web camera specifications

6.3.A Linearity check for the camera sensor used

It is vital that the web camera's sensor used in the experiment be checked for sensor linearity. Basically the non-linearity of any sensor indicates the deviation of the input-output relation from being a perfect straight line.

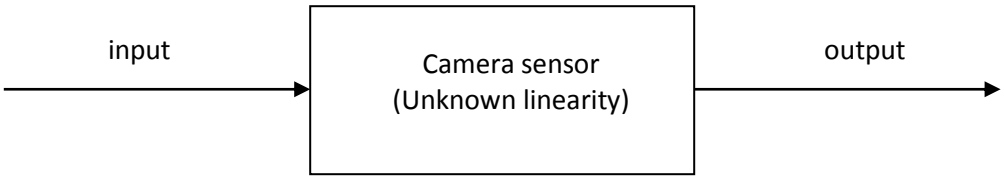

Figure 35 - Schematic of the camera sensor system.

To test for non-linearity, the output data of the sensor has to be obtained given a range of calibrated or well known exposure levels. This was achieved by using a changing light source and a predetermined fixed time of exposure to the sensor of the camera. This simple experiment was done at the Electrical Engineering Department Optics Lab.

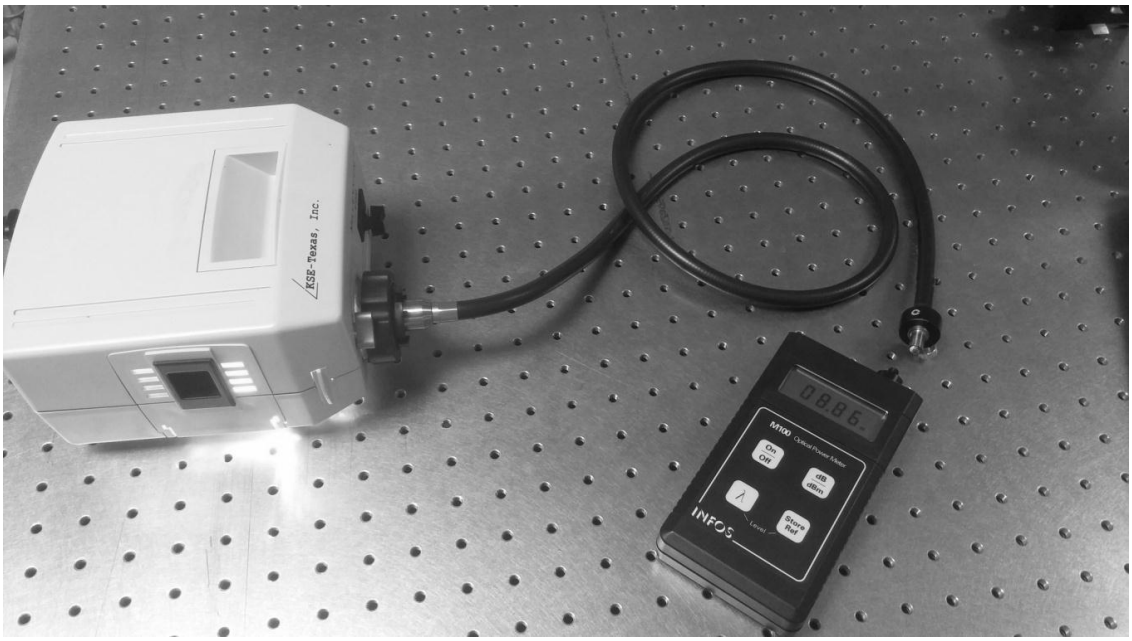

Figure 36 - The digital light meter and the light source used.

To confirm the linearity of the light source, the digital light meter above was used to record the intensity of the emitted light at different exposure levels (17 in this case).

The results are plotted below:

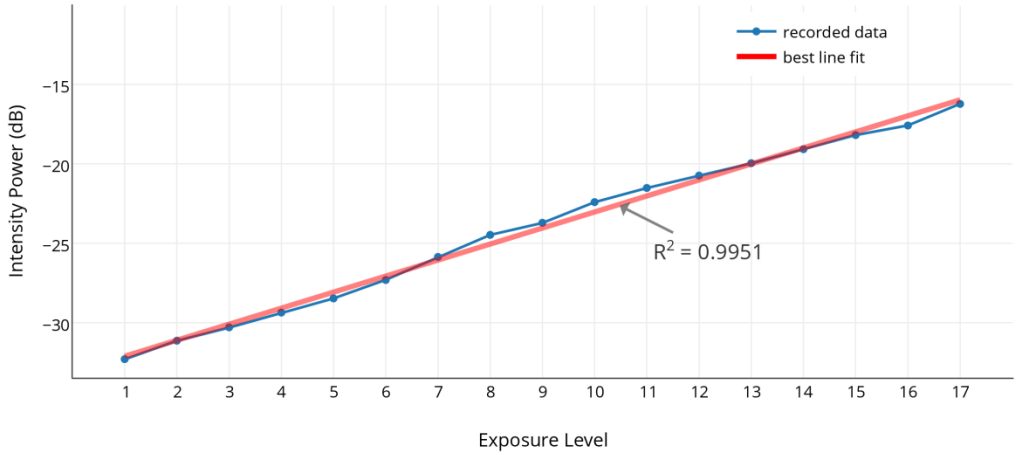

Figure 37 - Linearity response of the light source used.

The light source used can thus be confirmed to be linear itself and the next step is now to use the camera sensor to read the changing light exposure levels from the source.

For the 17 exposure levels, the camera sensor captured their images. It is important to note that a photographic filter was placed between the light source and the web camera to reduce the light intensity levels reaching the CMOS sensor inside the camera. The desired light intensity levels are the ones in the range of the light intensities recorded from the light sources during the dust storm events. Without the photographic filter, light intensities from the light meter would be too high and will not represent the real experiment conditions. The arrangement of the experiment was done as below then performed in dark room. A line of sight between the input light and the CMOS sensor of the web camera was perfectly established too.

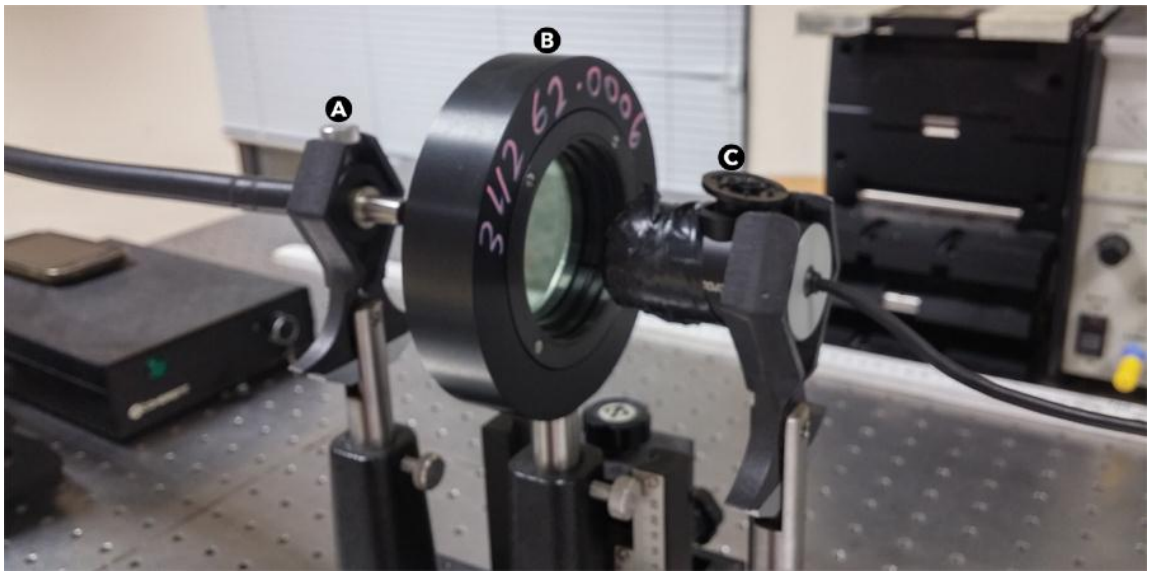

Figure 38 - Setup of the linearity test at optics laboratory. (**A**) Clip holding the input light source. (**B**) The photographic filter used to reduce the input light intensities. (**C**) The web camera being tested for linearity.

The captured images are shown below:

Figure 39 - The 17 captured images using the experiment setup in previous figure.

The captured images are then profiled to get their corresponding intensity values. The data was then plotted as below:

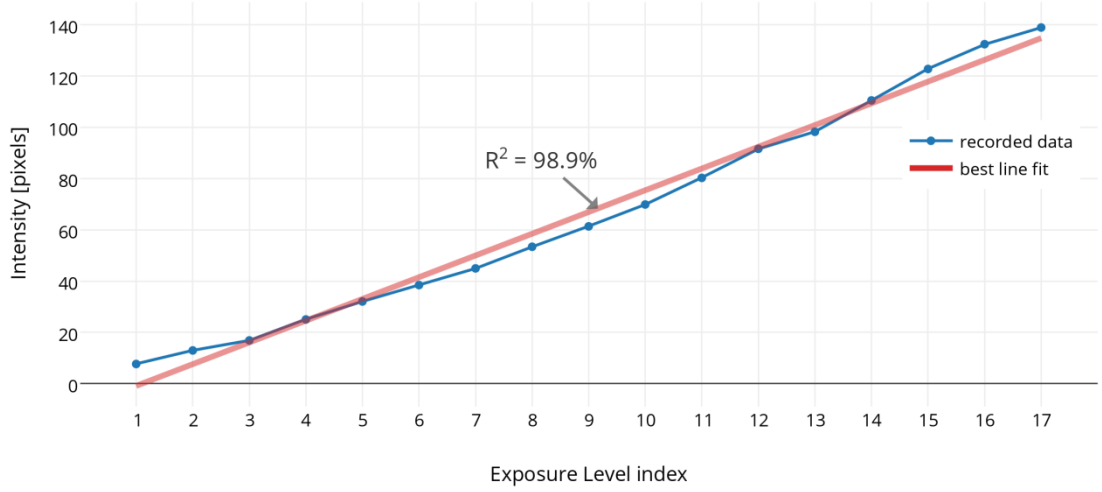

Figure 40 - Linearity response of the web camera used.

The fitting straight line fits the data with an R-squared value of 98.9%. This verifies that the web camera to be used is a linear device.

6.4 Experiment Site

The Khobar city area has abundant light point sources that can be useful as targets for this experiment. A reference is chosen that has a wide angle view of the entire Khobar region extending upto Bahrain. Lights from as far as Bahrain (approximately 30 Km away) are clearly visible during clear nights. The reference point chosen is from the top of KFUPM's building 5 where the telescope was placed for observations and recording of data.

In order to study the storm's dynamic physical structure, a specific region has to be selected to capture the light sources during a dust storm and in clear weather condition. For this work, the selection of the light sources followed the criterion below:

- They should be of same color (In this case orange street lights, approximate wavelength of 850nm)
- It is also preferable that they should be at same altitude (identical street lampposts)
- They should be at different distances from the observation location, spread across the horizon to investigate different regions of the storm.
- Since the observation is done by a single telescope, it is also preferable that the light sources be on the one side faced by the telescope and relatively close to each other as locating far spaced targets will be time consuming and one can miss important phases of the progressing dust storm.

The chosen region for observation extends from KFUPM traversing entire Khobar city and stretching all the way to the King Fahd causeway.

6.5 Observed Dust Storms

The figures below show Dhahran region from top of building 5 during a clear day and during a dust storm observed on 4 November 2014.

Figure 41 - Dust storm observed on 4 November 2014 in Dhahran area.

Figure 42 - Clear day in Dhahran 6 November 2014.

Table 8 summarizes all the observed dust storms:

DS#	Date	Approximate Duration	Approximate Start of Observation Time	Max. Wind Speed (Km/h)	Max. Relative Humidity (%)
DS1	04-11-2014	14:00 - 20:00 / 6 hrs	17:30	34	73
DS2	08-02-2015	17:00 - 22:00 / 5 hrs	18:00	27	82
DS3	22-02-2015	19:00 - 01:00 / 6 hrs	20:00	45	47
DS4	06-03-2015	18:00 - 22:00 / 4 hrs	19:00	48	59
DS5	01-04-2015	18:30 - 03:30 / 9 hrs	19:30	60	57

Table 8 - Summary of observed dust storms in the Dhahran region. Wind and relative humidity data from [34].

The technique of utilizing the telescope to capture the light sources was only practicable to be used after sun set.

A number of online weather prediction services were used to predict dust storm events. Some of them included [34]–[37]. They are not 100% reliable as sometimes they falsely predict dust storm events that never happen. For the purpose of research and observation, one has to be on standby at all times to capture this complex phenomenon.

The National Aeronautics and Space Administration (NASA) was also very useful in announcing major dust storm systems. Major news agencies would then broadcast alerts over the same. In Saudi Arabia, the government also sends SMS alerts for major and adverse dust storms through various mobile operators. These were all useful in tracking the dust storms.

The dust storm on 1 April 2015 was the worst of the year 2015 so far reducing visibility to 'near zero' as reported by [38]. By the next day (2 April 2015), the storm had swept many parts of the gulf region moving southwards to Yemen and Oman as shown by the NASA's released satellite picture below:

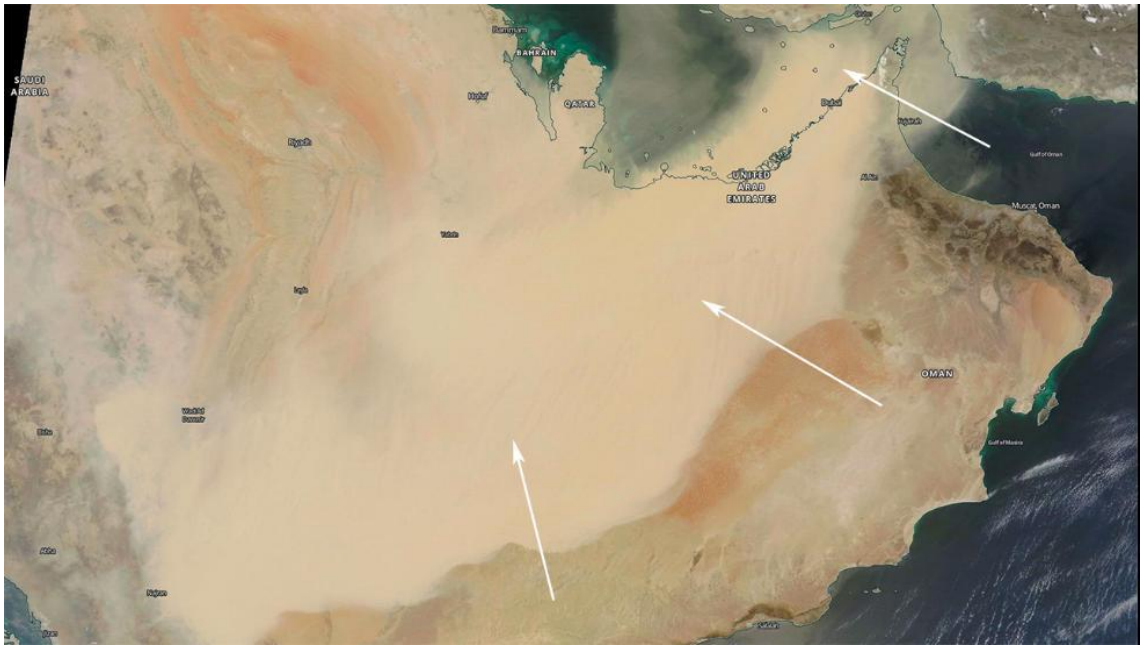

Figure 43 - April 2, 2015 Dust storm sweeping over the Gulf region as captured by one of the NASA satellite. The largest areas of the storm are shown with the arrows [38].

6.6 Data Analysis

The schematic below shows how the analysis was undertaken:

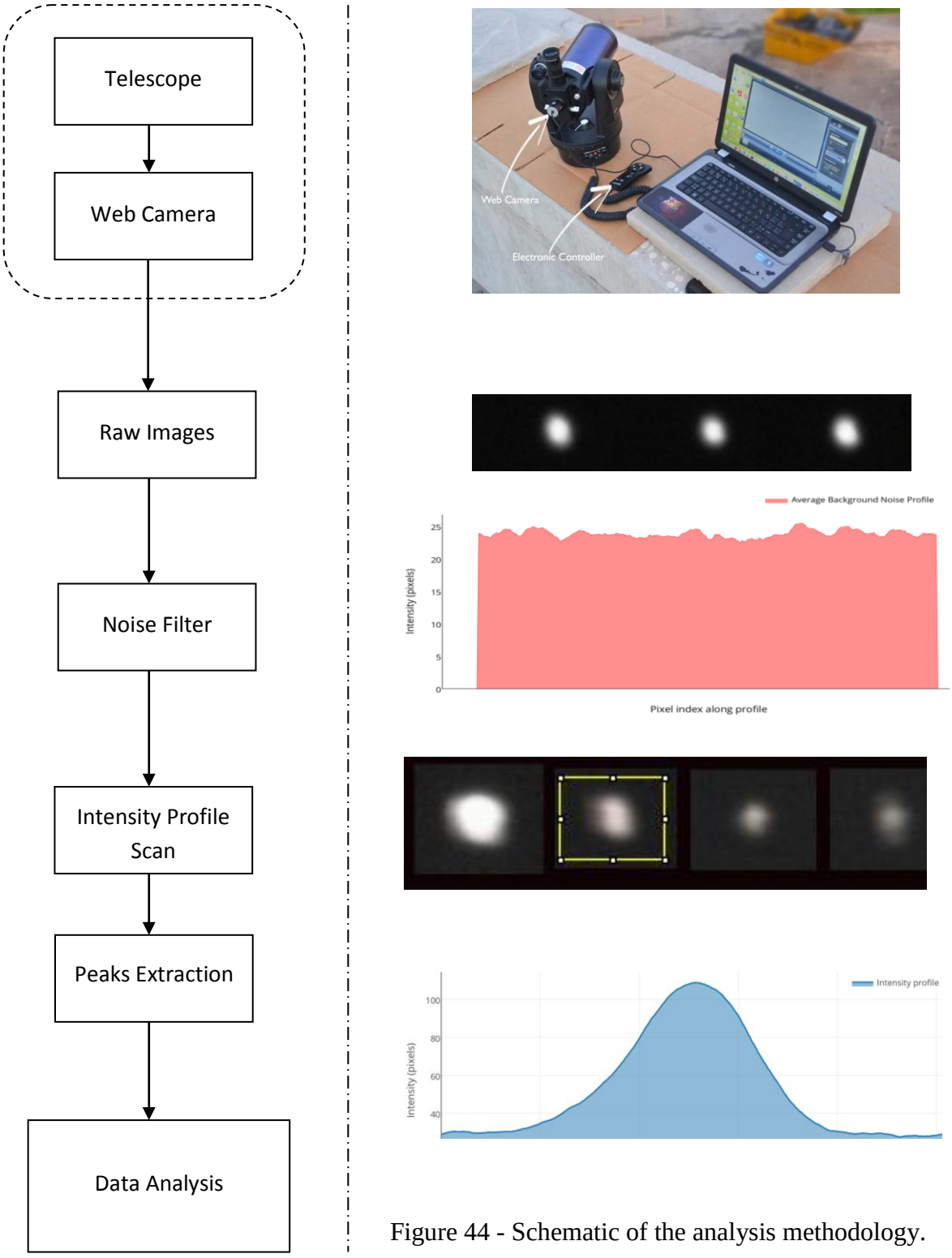

Figure 44 - Schematic of the analysis methodology.

6.6.A Background Noise Profile

It is vital to eliminate any form of background noise in the image profile data before proceeding to the next stages. The background noise was obtained by pointing the telescope at nothing (dark area) and raw images captured over time. The raw images are then scanned for intensity profiles and averaged over the pixel indexes and over time. The average background noise profile is shown below:

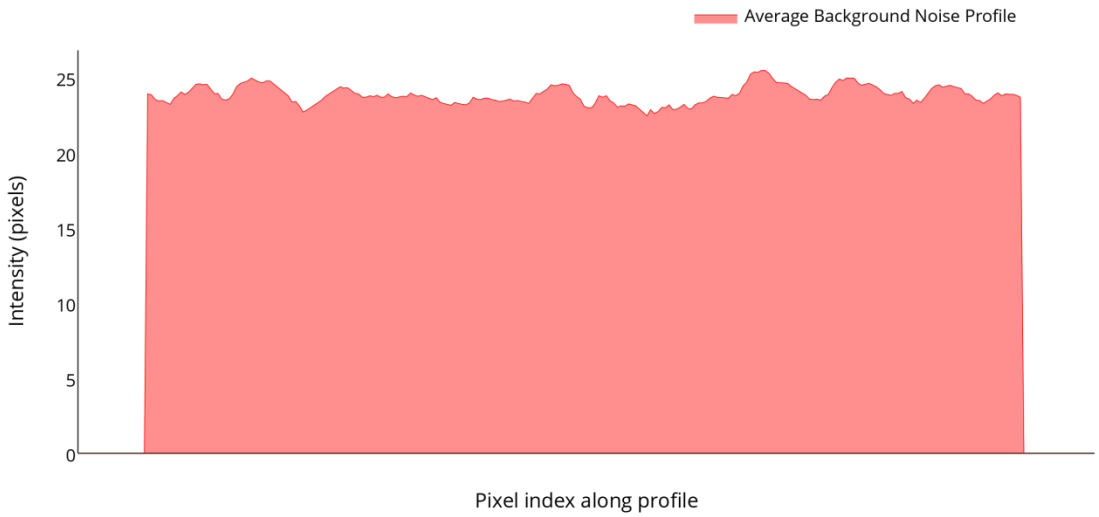

Figure 45 - The intensity profile for the average background noise.

An average value of 25 representing the background noise was therefore deducted from all upcoming profile statistics.

6.6.B Targets Intensity Profile

The targets are compiled from the raw images and scanned for profiling of their intensities. A total of 12 targets spread over the city's horizon were recorded during image data acquisition. Light sources beyond the city towards Bahrain were extremely difficult to be targeted during dust storm events. For the worst storm observed on 1 April

2015, only 2 targets closest to the observation point were visible and were recorded. The extremely reduced visibility made it impossible to capture any other targets. The table below shows the final extracted pixel values for the dust storms observed.

Target #	Distance from Telescope, L_C [Km]	DS1	DS2	DS3	DS4	DS5
1	1.9	129.7	109.6	111.4	110.8	28.7
2	2.29	99.6	98.6	86.8	77.9	21.7
3	4.22	83.1	77.3	74	67.5	-
4	5.33	68.4	68.7	48.3	62.7	-
5	5.89	48.8	56.7	39.3	50.1	-
6	6.54	41.2	47.9	31.8	44.2	-
7	7.18	34.4	34.8	27.9	35.8	-
8	7.43	32.7	32.3	25.8	28.3	-
9	7.83	28.6	31.7	21.4	25.1	-
10	9.64	21.9	30.3	19.2	24.7	-
11	10.34	17.5	29.5	16.9	24.3	-
12	15.54	12.4	27.8	14.1	17.8	-

Table 9 - The extracted intensity pixel values [0-255] shown in shaded cells, sorted by the distances to the observation point.

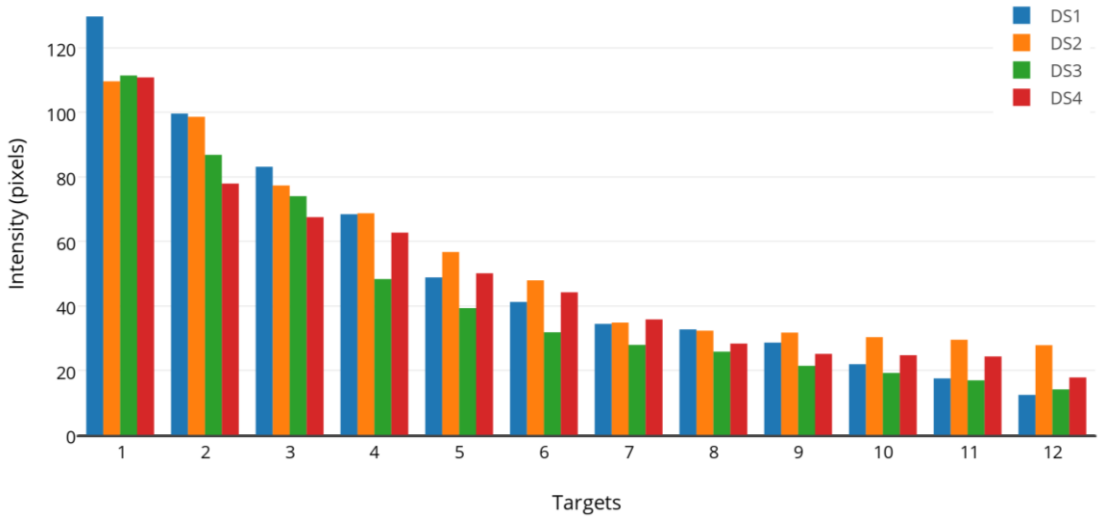

Figure 46 - Bar chart compares at a glance the extracted profiles of the observed storms.

For the individual dust storms, the following graph shows the recorded light intensities over the studied region. The pixel data is plotted against the real coordinate location of the targets from the observation point.

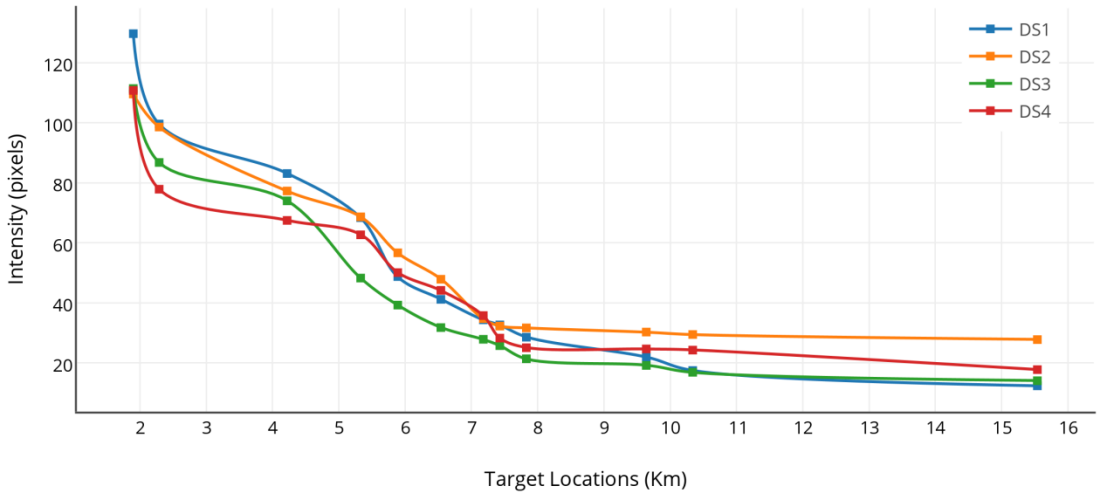

Figure 47 - Intensity profiles for all observed dust storms verses real target locations.

The dust storm DS5 data is not shown here as only the first 2 targets were visible during that particular dust storm event.

Analysis of the recorded target light intensities follows now.

6.6.C Analysis and Discussion

In this sub-section, the data extracted from the previous section is further analyzed and discussed to shade light on the implications of the storm's dynamic structure.

The following model shall be used to illustrate the idea:

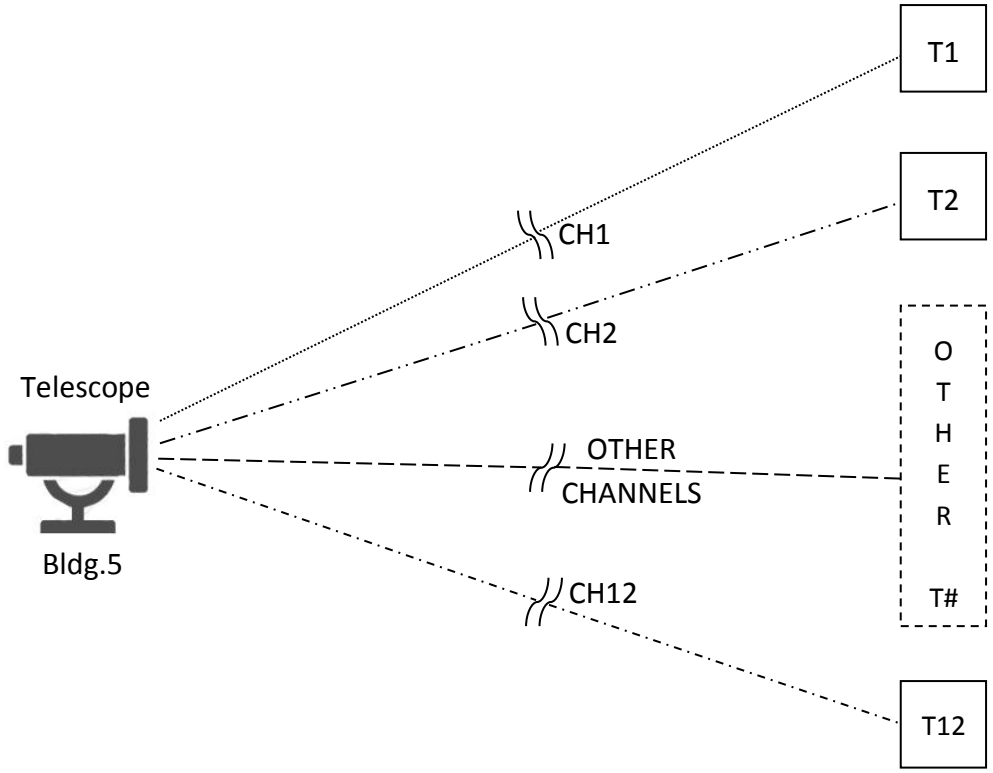

Figure 48 - Schematic of the experiment configuration, the targets are non-equidistant from the telescope.

The channel lengths L_C, are as given in Table 9 or for easier referencing tabulated below:

Target No.	1	2	3	4	5	6	7	8	9	10	11	12
Distance from Telescope, L_C [Km]	1.9	2.29	4.22	5.33	5.89	6.54	7.18	7.43	7.83	9.64	10.3	15.5

Table 10 - Corresponding distances of the light sources observed from the telescope.

Since the observations are done using a single telescope from the same point, the configuration above shows the light targets T1, T2 upto T12 and their corresponding virtual channels CH1, CH2 upto CH12 spread over the observation area of Dhahran city.

The intensities of each target was recorded for a clear day (dust-free) and during the dust storm events observed. The drop in intensities during the dust storms is solely due to the presence of dust. With the channels being independent of each other, we can investigate the variation of dust concentration over each of them individually.

To investigate this, the dust storms data is processed and dust attenuation factors (*DAF*) for individual targets due to the DUSA effect in each channel calculated as shown below:

$$DAF_T = \frac{Target\ Light\ Intensity\ on\ Clear\ Day\ (TLI_C)}{Target\ Light\ Intensity\ on\ Dusty\ Day\ (TLI_D)} \qquad \textbf{(22)}$$

The subscripts *D* and *C* on the target light intensities distinguishes the clear (TLI_C) and the channel (TLI_D). The subscript *T* on the dust attenuation factor indicates that it is for the targets (DAF_T).

The extent of the attenuation is now expressed in decibels as follows:

$$Attenuation = 10\,log(DAF_T) \qquad [dB] \qquad \textbf{(23)}$$

Using equation (23) and the channel lengths, L_C from Table 10, we can compute the corresponding attenuation per unit distance on each of the channels as follows:

$$Channel\ Attenuation\ per\ unit\ distance = \frac{10\,log(DAF_T)}{L_C} \qquad [dB/Km] \qquad \textbf{(24)}$$

Using equations (22), (23) and (24) the following data in Table 11 is generated by a standard excel sheet.

Targets, T#	T1	T2	T3	T4	T5	T6	T7	T8	T9	T10	T11	T12
Channel Length (Lc)	1.9	2.29	4.22	5.33	5.89	6.54	7.18	7.43	7.83	9.64	10.34	15.54
Clear Intensity	141.9	132	123.6	85.6	73.3	65.9	63	49.8	38.3	36.4	31.7	28.7
Dust Storm 1	129.7	99.6	83.1	68.4	48.8	41.2	34.4	32.7	28.6	21.9	17.5	12.4
Dust Storm 2	109.6	98.6	77.3	68.7	56.7	47.9	34.8	32.3	31.7	30.3	29.5	27.8
Dust Storm 3	114.4	86.8	74	48.3	39.3	31.8	27.9	25.8	21.4	19.2	16.9	14.1
Dust Storm 4	110.8	77.9	67.5	62.7	50.1	44.2	35.8	28.3	25.1	24.7	24.3	17.8
Using DS1 Data												
Dust Attn. Eq22	0.3904	1.2231	1.7242	0.9742	1.7668	2.0399	2.6278	1.8268	1.2683	2.2066	2.5802	3.6446
Dust Attn/Dist. Eq23	0.2055	0.5341	0.4086	0.1828	0.3	0.3119	0.366	0.2459	0.162	0.2289	0.2495	0.2345
Using DS2 Data												
Dust Attn. Eq22	1.1217	1.267	2.0384	0.9552	1.1152	1.3855	2.5776	1.8803	0.8214	0.7966	0.3124	0.1384
Dust Attn/Dist. Eq23	0.5904	0.5533	0.483	0.1792	0.1893	0.2119	0.359	0.2531	0.1049	0.0826	0.0302	0.0089
Using DS3 Data												
Dust Attn. Eq22	0.9356	1.8205	2.2279	2.4853	2.7071	3.1646	3.5374	2.8561	2.5279	2.778	2.7317	3.0866
Dust Attn/Dist. Eq23	0.4924	0.795	0.5279	0.4663	0.4596	0.4839	0.4927	0.3844	0.3228	0.2882	0.2642	0.1986
Using DS4 Data												
Dust Attn. Eq22	1.0744	2.2904	2.6271	1.3521	1.6527	1.7346	2.4546	2.4544	1.8353	1.684	1.1545	2.0746
Dust Attn/Dist. Eq23	0.5655	1.0002	0.6225	0.2537	0.2806	0.2652	0.3419	0.3303	0.2344	0.1747	0.1117	0.1335

Table 11 - Processed dust storm data using equations (23) and (24).

Using the channel attenuation data from the above table, the following charts are plotted to show the channel behavior due to dust attenuation for all the storms observed.

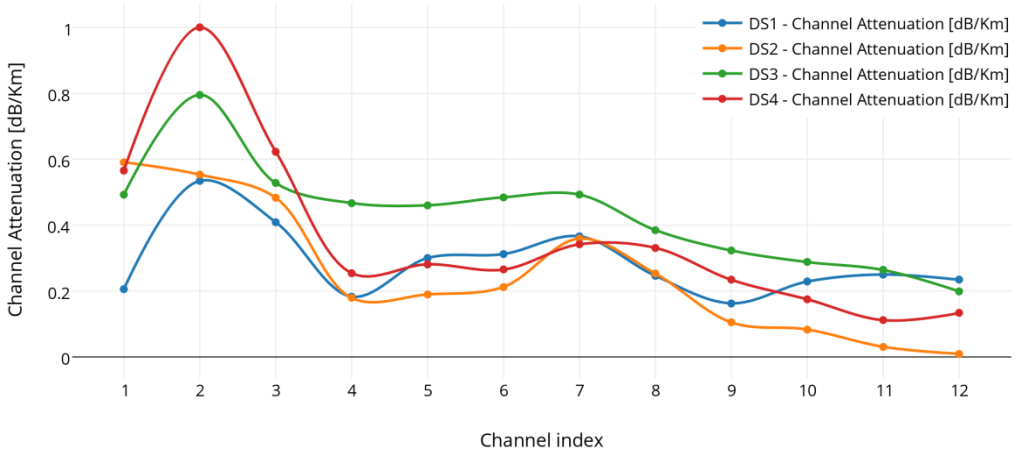

Figure 49 - Channel attenuation data for all observed DUSA storms

For the individual storms, the following charts and remarks can be deduced:

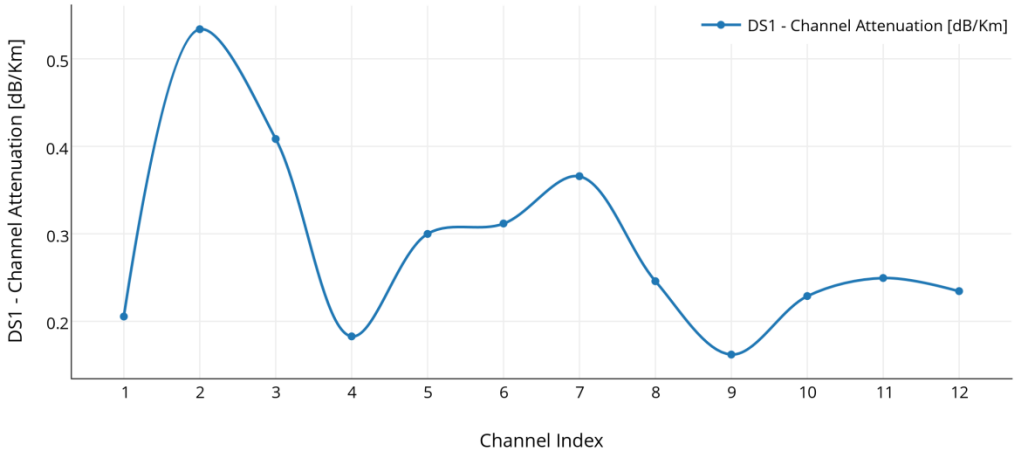

Figure 50 - DS1 channel attenuation behavior

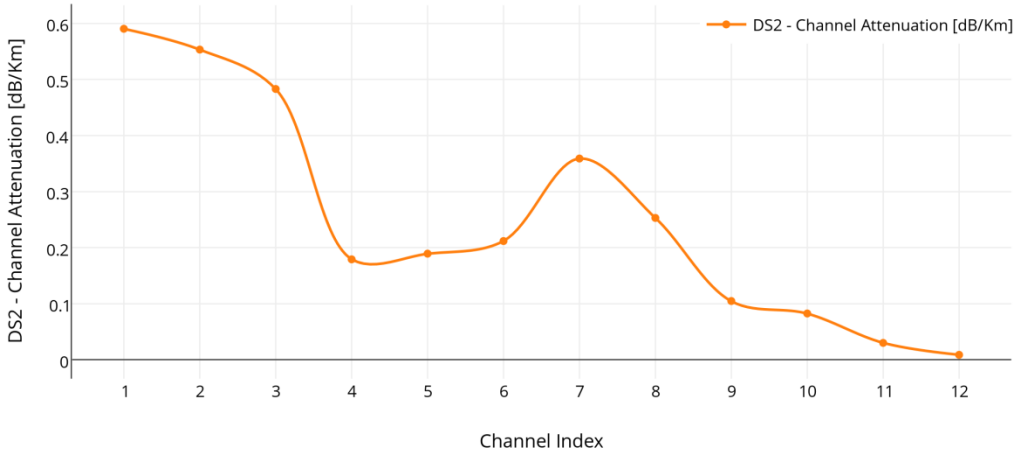

Figure 51 - DS2 channel attenuation behavior

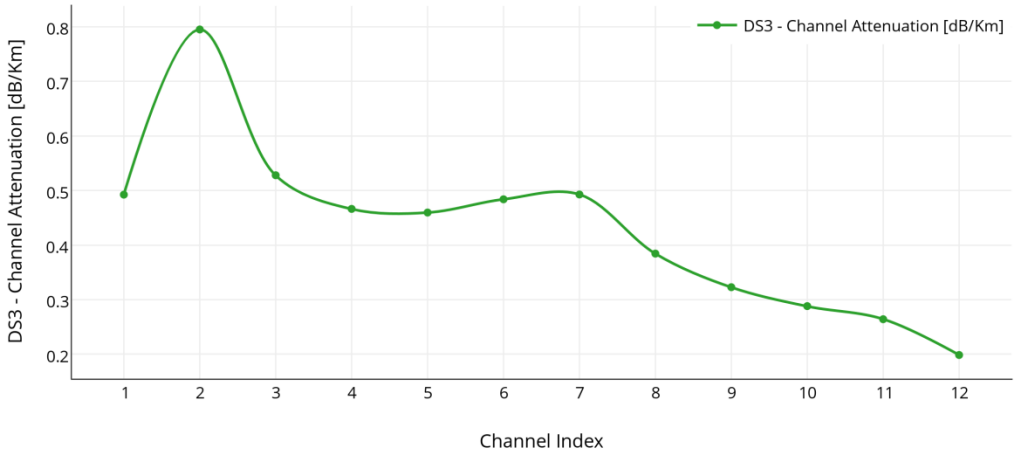

Figure 52 - DS3 channel attenuation behavior

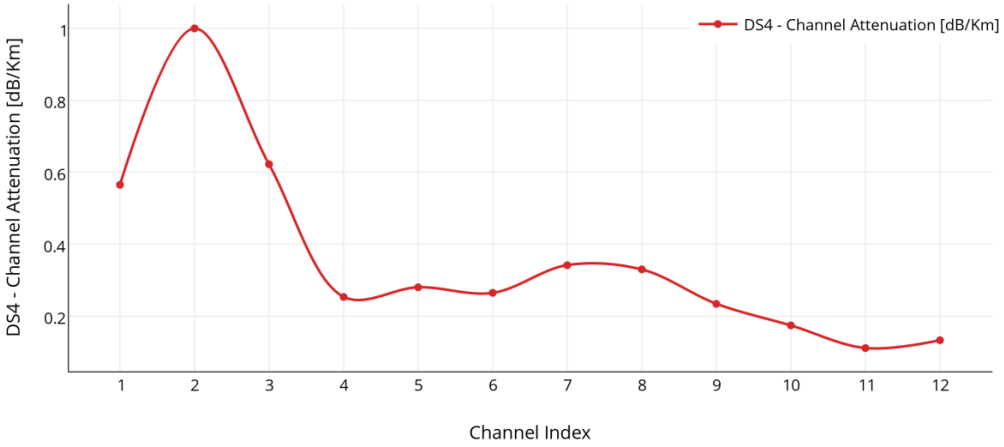

Figure 53 - DS4 channel attenuation behavior

Comments and remarks:

- It is observed during the 4 observed dust storms that dust intensity is not uniform in the region of observation as in specific regions of the city dust caused attenuation as high as 1 dB/Km while other regions experienced dust intensities that resulted in attenuations as low as 0.008 dB/Km.
- There were regions in the observation area that were generally experiencing higher dust attenuations during all the 4 dust storms. This could be attributed to having no surrounding buildings and therefore not being shielded from dust while other regions had low dust attenuation levels.

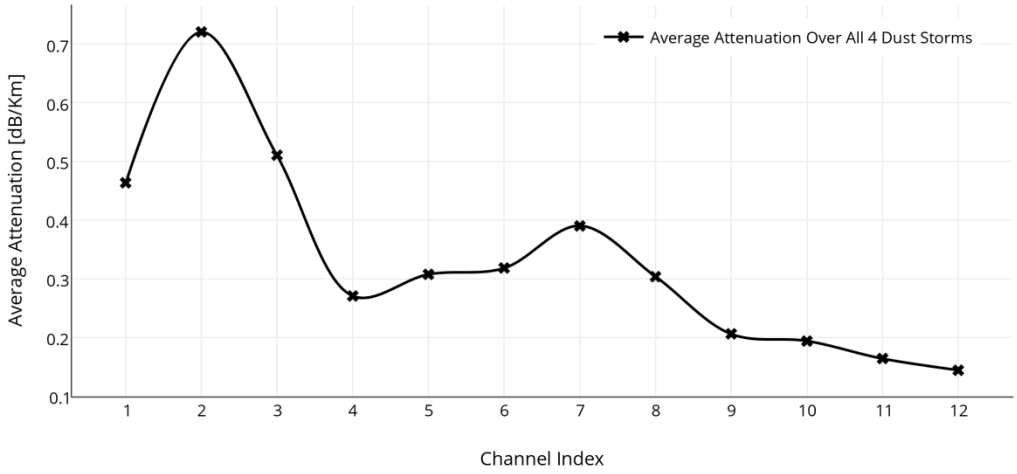

Figure 54 - Averaged attenuation over all the 4 observed dust storms

- A paramount conclusion is that layering in the horizontal expanse of the dust storms clearly exist and is observed with clarity in the experiment.
- Although this experiment is conducted in a city environment, it is expected the same would also occur in desert as surrounding sand dunes may have the same effect of buildings in a city.

The implication of the above behavior on the horizontal expanse of the storm has a profound impact on how mitigation of the dust effects can be implemented.

Real time knowledge of the channels can be used to intelligently and adaptively mitigate the dust effects between practical nodes in a network system.

Considering the 12 channel lengths of the experiment configuration to be real communication path links in a GSM core base station sub-system, where the telescope position is taken by a base station controller (BSC) and the light targets being the base transceiver stations (BTS), a service provider can use the dynamic channel information to control how dust attenuation effects can be mitigated more effectively.

Instead of compensating for a fixed channel attenuation due to dust, a smart approach can be utilized once the channel information is known in real time.

In practice, one solution that can be suggested is to employ sensors along such terrestrial microwave communication networks to estimate the general model of the storm as it progresses.

The data from such sensors can in turn be used to adaptively alter transmission parameters to precisely suit the channel problem due to dust storms.

In that way for example, the transmit power will be spent effectively leading to a more cost-effective communication system that is reliable and robust at any given environmental condition.

6.7 Limitations of the Experiment Technique

This section highlights some of the major challenges and limitations of the experimental work technique.

The first challenge is the unreliability of weather prediction systems to perfectly predict the advent of a dust storm event. Currently there are no meteorological systems in place in the region dedicated to dust storm prediction. Beyond the Gulf region, international weather advisory systems exist but also cannot ultimately predict with utmost certainty of impending dust storms enveloping the region.

For example, the Northern Africa-Middle East-Europe (NA-ME-E) is a world meteorological organization's (WMO) program for sand and dust storm warning advisory and assessment system (SDS-WAS). The system doesn't provide forecast information beyond the current day's. Inability to have this information for future upcoming dust events is not an ideal situation for research based on the dust storms. As researchers it is vital to be able to have credible information regarding the phenomenon one is observing and tracking. The time one would take measurements is vital in this research, a delay in taking measurements relative to start of a dust storm would result in having dust mix-up. This makes the study of the dust storm behavior more difficult under such circumstances.

The other limitation in respect to the chosen methodology for this work entails the inability to observe the light sources and take the measurements during the day. Capturing any light source will be impossible with ambient sun light adding high amounts of noise that would overwhelm the light from target sources. In addition, the light sources themselves are usually off during the day. It was only practical to do

observations after sun set. A novel technique that can observe and study the dust storm at any given time would be ideal for the expansion of this work. One of such ideas has been suggested in the future work section of this report.

A third point is the difficulty associated with focusing the single telescope on spread targets especially during a dust storm. The much reduce

d visibility added difficulty in the telescope maneuvers and fine tunings in finding the chosen targets one after the other for observation and data recording. A more better configuration would have been to have multiple telescopes fixed on their targets and doing observations simultaneously.

7. Conclusion

The study involved an extensive review of parameters in literature contributing to the physical model of the dust storms and their impacts on the attenuation effects to microwave signals. Also extending from existing methods of approximating dust storm models on the vertical expanse, the horizontal expanse of the storm is modeled. The simpler model was derived from a layering concept studied before from literature.

A real downlink of a NanoSAT was redesigned considering the dust attenuation parameter. The undertaken downlink analysis was found to have an optimum desirable link margin leading to a cost-effective operation in case of impairments due to channel degraders including dust and sand storms. This is very critical especially for miniaturized satellites which have payload weight challenges. The minimal power available in such satellites needs to budgeted and used effectively with all possible meteorological problems taken into account. As such, the dust attenuation parameter inclusion in the downlink redesign is of utmost significance.

An extensive analysis of dust storm data from WMO was done and can reliably provide a guide to system engineers designing microwave links, specifically the terrestrial links, when computing and estimating link budgets for their systems with regards to the dust attenuation parameter. In essence, this will enable setting early plans to pre-mitigate the severe effects caused by DUSA storms on their microwave powered links.

The observed dust storms maybe few as at the time this report is published due to a number of factors stated in the previous section, however, the current results directs the future expansion of the work to further investigate this complex phenomenon.

The experimental findings shows that the horizontal virtual layers of visibility actually exist as can be clearly seen from the virtual channels with varying point attenuations. The dusty medium along the horizontal expanse exhibits differences in dust concentration making visibilities to vary accordingly.

Moving forward from this work and studying the storm's behavior on a much larger scale with an improved technique and advanced equipment, the findings will go further in improving the theoretical models describing and predicting future storm effects on radio communication.

In a real communication system therefore, the idea of individually estimating the channel path attenuation due to dust in a microwave network having several nodes under dusty conditions is vital in utilizing the resources effectively, rather than mitigating based on a fixed power level for the entire region of radio coverage. This translates to less expenditure on power, making the radio links more robust and cost effective under dusty channel environments.

7.1 Future Work

A new methodology to study the horizontal expanse of the dust storm on a larger scale needs to be developed in the future in form of a funded research project by the current author.

With the current available equipment and resources, the study area was a relatively smaller region and a more sophisticated technique needs to be devised to study storm structures more effectively without the current limitations. However the current work done was crucial for the next step in the research of this complex phenomenon.

Among the preliminary ideas regarding the new technique include the use of high powered lasers to be setup along a certain stretch (e.g. 50 -100 Km) of a major highway crossing over a desert region near one of the dust storm hot spots in Saudi Arabia. Having the equipment in place and ready for the storms, the recorded data would then be remotely sent to a terminal back at the laboratory for processing and analysis. The expanded scale of the study will provide a clearer picture of the dust storm behavior, structure and characteristics vital in the search for perfection of the theoretical models proposed earlier.

Another useful item that can be done in future is having a complete generic 3D model of dust storm that can be used by a practical telecommunication system to give accurate attenuation figures once a dust storm epicenter is detected and the direction and speed of prevailing winds is predicted. This will give service providers an opportunity for them to be fully prepared to respond to dust storm outages thereby minimizing the effects of the dust storms on their microwave powered networks.

As part of the extension of the terrestrial DUSA outage planning, a similar analysis shall be done to include planning for satellite links. A number of data parameters are readily available at the WMO's BDFC center which can be utilized to create a model for dust outage planning involving satellite powered microwave links.

New discoveries and advancements in this line of research will be helpful for current and future microwave based communications in arid and semi-arid regions of the world.

REFERENCES

[1] C. S. Bristow, K. A. Hudson- Edwards, and A. Chappell, "Fertilizing the Amazon and equatorial Atlantic with West African dust," *Geophys. Res. Lett.*, vol. 37, no. 14, 2010.

[2] K. Harb, B. Omair, S. Abdul-Jauwad, A. Al-Yami, and A. Al-Yami, "A proposed method for dust and sand storms effect on satellite communication networks," *Innov. Commun. Theory INCT*, vol. 12, 2012.

[3] A. Safaai-Jazi, H. Ajaz, and W. L. Stutzman, "Empirical models for rain fade time on Ku- and Ka-band satellite links," *IEEE Trans. Antennas Propag.*, vol. 43, no. 12, pp. 1411–1415, Dec. 1995.

[4] M. S. J. Singh, S. I. S. Hassan, M. F. Ain, K. Igarashi, K. Tanaka, and M. Iida, "Proposed Rain Attenuation Model Revised from ITU Used for Prediction in Tropical Climates," in *2005 Fifth International Conference on Information, Communications and Signal Processing*, 2005, pp. 994–996.

[5] K. Harb, O. Butt, A. A. Al-Yami, and S. Abdul-Jauwad, "Probabilistic dust storm layers impacting satellite communications," in *Space Science and Communication (IconSpace), 2013 IEEE International Conference on*, 2013, pp. 407–411.

[6] K. Harb, C. Huang, A. Srinivasan, and B. Cheng, "Intelligent Weather Systems with Fuzzy Logic Controller for Satellite Networks," in *IEEE Wireless Communications and Networking Conference, 2008. WCNC 2008*, 2008, pp. 3069–3074.

[7] The-COMET-Program, "Atmospheric dust module," http : //www.meted.ucar.edu/eumetsat/at dust/ Available Online, last accessed date Feb. 2015.

[8] K. Afzaal, T. K. Bandopadhyaya, and S. Poonam, "Effect of soil textural class and relative humidity of regions in accurate prediction of attenuation of millimeter waves during sand and dust storms," in *Physics and Engineering of Millimeter and Sub-Millimeter Waves, 2001. The Fourth International Kharkov Symposium on*, 2001, vol. 1, pp. 393–395.

[9] R. A. Bagnold, *The physics of blown sand and desert dunes*. Courier Corporation, 2012.

[10] S. I. Ghobrial, I. A. Ali, and H. M. Hussein, "Microwave attenuation in sand storms," in *Int. Symp. Antennas Propagat., Sendai, Japan*, 1978.

[11] A. Ansari and B. G. Evans, "Microwave propagation in sand and dust storms," in *IEE Proceedings F (Communications, Radar and Signal Processing)*, 1982, vol. 129, pp. 315–322.

[12] C. S. Zender, H. Bian, and D. Newman, "Mineral Dust Entrainment and Deposition (DEAD) model: Description and 1990s dust climatology," *J. Geophys. Res. Atmospheres 1984–2012*, vol. 108, no. D14, 2003.

[13] S. I. Ghobrial and S. Sharief, "Microwave attenuation and cross polarization in dust storms," *IEEE Trans. Antennas Propag.*, vol. 35, no. 4, pp. 418–425, Apr. 1987.

[14] Q. Dong, Y.-L. Li, J. Xu, H. Zhang, and M. Wang, "Effect of Sand and Dust Storms on Microwave Propagation," *IEEE Trans. Antennas Propag.*, vol. 61, no. 2, pp. 910–916, 2013.

[15] A. R. V. Hippel, *Dielectric materials and applications*. Artech House, 1954.

[16] E. G. Njoku and J.-A. Kong, “Theory for passive microwave remote sensing of near-surface soil moisture,” *J. Geophys. Res.*, vol. 82, no. 20, pp. 3108–3118, Jul. 1977.
[17] T. Schmugge, P. Gloersen, T. Wilheit, and F. Geiger, “Remote sensing of soil moisture with microwave radiometers,” *J. Geophys. Res.*, vol. 79, no. 2, pp. 317–323, Jan. 1974.
[18] J. Wang, T. Schmugge, and D. Williams, *Dielectric constants of soils at microwave frequencies-2*. 1978.
[19] S. Sharif, “Chemical and mineral composition of dust and its effect on the dielectric constant,” *IEEE Trans. Geosci. Remote Sens.*, vol. 33, no. 2, pp. 353–359, Mar. 1995.
[20] S. I. Ghobrial and S. M. Sharif, “Measurement of the dielectric constant of dust at 8.3 GHz,” in *National Radio Science Meeting*, 1982.
[21] M. A. Alhaider and A. A. Ali, “Experimental studies on millimeterwave and infrared propagation in arid land: The effect of sand storms,” in *Antennas and Propagation, 1989. ICAP 89., Sixth International Conference on (Conf. Publ. No. 301)*, 1989, pp. 268–270.
[22] K. Harb, O. Butt, S. Abdul-Jauwad, and A. M. Al-Yami, “Systems Adaptation for Satellite Signal under Dust, Sand and Gaseous Attenuations,” *J. Wirel. Netw. Commun.*, vol. 3, no. 3, pp. 39–49, 2013.
[23] J. Goldhirsh, “Attenuation and backscatter from a derived two-dimensional duststorm model,” *Antennas Propag. IEEE Trans. On*, vol. 49, no. 12, pp. 1703–1711, 2001.
[24] E. A. A. Elsheikh, M. R. Islam, K. Al-Khateeb, A. H. M. Z. Alam, and Z. O. Elshaikh, “A proposed vertical path adjustment factor for dust storm attenuation prediction,” in *Mechatronics (ICOM), 2011 4th International Conference On*, 2011, pp. 1–3.
[25] Z. Elabdin, M. R. Islam, O. O. Khalifa, and A. F. Ismail, “Duststorm measurements for the prediction of attenuation on microwave signals in Sudan,” in *Computer and Communication Engineering, 2008. ICCCE 2008. International Conference on*, 2008, pp. 1181–1185.
[26] E. A. Elsheikh, M. R. Islam, A. Z. Alam, A. F. Ismail, K. Al-Khateeb, and Z. Elabdin, “The effect of particle size distributions on dust storm attenuation prediction for microwave propagation,” in *Computer and Communication Engineering (ICCCE), 2010 International Conference on*, 2010, pp. 1–5.
[27] K. Harb, S. Abdillah, and S. Abdul-Jauwad, “Dust amp; sand (DUSA) storms impact on LEO satellite microwave radio links,” in *Advanced Satellite Multimedia Systems Conference and the 13th Signal Processing for Space Communications Workshop (ASMS/SPSC), 2014 7th*, 2014, pp. 442–447.
[28] A. Arun and T. K. Sreeja, “An effective downlink budget for 2.24GHz S-Band LEO satellites,” in *2013 IEEE Conference on Information Communication Technologies (ICT)*, 2013, pp. 342–345.
[29] M. Hamidi, M. R. Kavianpour, and Y. Shao, “Synoptic analysis of dust storms in the Middle East,” *Asia-Pac. J. Atmospheric Sci.*, vol. 49, no. 3, pp. 279–286, 2013.

[30] "Dust Surface Concentration — Barcelona Dust Forecast Center." [Online]. Available: http://dust.aemet.es/forecast/nmmb-bsc-dust-forecast-sconc. [Accessed: 24-Jun-2015].
[31] Y. Shao, *Physics and Modelling of Wind Erosion*. Springer Science & Business Media, 2008.
[32] S. Sharif, "Clutter and backscatter cross-section of dust storms at X-band," *Sudan Eng. Soc. J.*, vol. 44, no. 35, pp. 58–70, 1997.
[33] E. M. Abuhdima and I. M. Saleh, "Effect of sand and dust storms on GSM coverage signal in southern Libya," in *2010 Intl Conf on Electronic Devices, Systems and Applications (ICEDSA)*, 2010, pp. 264–268.
[34] "Weather History & Data Archive | Weather Underground." [Online]. Available: http://www.wunderground.com/history/. [Accessed: 11-Apr-2015].
[35] "Historical Weather For The Last Twelve Months in Dammam, Saudi Arabia - WeatherSpark." [Online]. Available: https://weatherspark.com/history/32759/2015/Dammam-Eastern-Province-Saudi-Arabia. [Accessed: 11-Apr-2015].
[36] "Yahoo Weather - Weather Forecasts | Maps | News," *Yahoo Weather*. [Online]. Available: https://weather.yahoo.com/. [Accessed: 24-Apr-2015].
[37] "NASA - Weather Information." [Online]. Available: http://www.nasa.gov/centers/kennedy/news/weather.html. [Accessed: 24-Apr-2015].
[38] "Major Dust Storm Hits Middle East, Impacts Travel and Air Quality, and Turns the Sky Bright Orange," *The Weather Channel*. [Online]. Available: http://www.weather.com/news/news/middle-east-sandstorm-saudi-arabia-qatar-dubai?_escaped_fragment_. [Accessed: 11-Apr-2015].

VITAE

Name: SAID ABDILLAH SAID

Nationality: KENYAN

Date of Birth: 2 FEB 1987

Email: g201203520@kfupm.edu.sa

said87abdill@gmail.com

Address KSA: King Fahd University of Petroleum & Minerals (KFUPM)

Address Kenya: Majengo, Mombasa, Kenya.

Academic Background:

Primary:	Mambrui Primary School, Mambrui, Kenya.
Secondary:	Sheikh Khalifa Bin Zayed Al-Nahyan, Mombasa, Kenya.
Undergraduate:	Kenyatta University, Nairobi, Kenya.
Postgraduate:	King Fahd University of Petroleum & Minerals (KFUPM), Dhahran, Saudi Arabia.

2014 7th Advanced Satellite Multimedia Systems Conference and the 13th Signal Processing for Space Communications Workshop (ASMS/SPSC)

Dust & Sand (DUSA) Storms Impact on LEO Satellite Microwave Radio Links

Kamal Harb[1], Said Abdillah[2], Samir Abdul-Jauwad[3]
Electrical Engineering Department, KFUPM University
Dhahran 31261, Saudi Arabia
Email: 1- kharb@kfupm.edu.sa; 2- g201203520@kfupm.edu.sa; 3- samara@kfupm.edu.sa

***Abstract*—Satellite telecommunications today present one of the most remarkable opportunities as they enable us to communicate and virtually reach any corner of the world. Great discoveries and developments in this field have enabled us to improve our quality of life. But even as we benefit from this progress, many challenges are encountered as satellite service providers uphold certain quality of service (QoS) levels. Meteorological impairments will always confront the satellite telecommunication links. Arid and semi-arid regions are particularly prone to dust and sand (DUSA) storms posing a looming threat to microwave radio systems reliability. A novel approach to model the dust storms in a three dimensional space has been presented and elaborated here leading to a more efficient attenuation computation and ultimately resulting in perfection of link budget design. A real downlink improvement for a LEO satellite will be re-designed by considering the dust attenuation parameter. An interesting finding is then confirmed that after including the dust attenuation parameter the link margin is found to be in healthy acceptable range and cost effective too. In order to have an efficient communication system and better quality of service (QoS), designers need to consider all the parameters that can impact communication link.**

***Index Terms*—Dust and Sand (DUSA) Storms, Particle Size Distribution (PSD), Signal to Noise Ratio (SNR), Quality of Service (QoS), Visibility.**

I. Introduction

Scientific findings have lately revealed that atmospheric dust and sand (DUSA) blowing off from vast central African deserts and the Middle East to the basin of the Amazon compensates for poor rainforest soils [1]. As the DUSA plumes nourishes the ecological systems of the world, they concomitantly pose a big threat to wireless communication systems, both terrestrial and satellite, by hampering them through degradation of the microwaves. Other meteorological circumstances similarly play a significant role in causing propagation impairments on satellite systems. Severe cases can cause total satellite link unavailability [2].

The microwave spectrum is quickly being filled up as wireless and satellite networks for broadband multimedia communications are being widely deployed all over the world. This has motivated a lot of research in designing efficient satellite-earth communication systems. The focus has been on the free-space channel and understanding the effects in terms of signal attenuation of particles like rain, snow, sand and dust (DUSA) present at some points along the satellite channel depending on region of operation. The scenarios get worse as higher frequency bands (Ku and Ka) are approached and beyond their ambit.

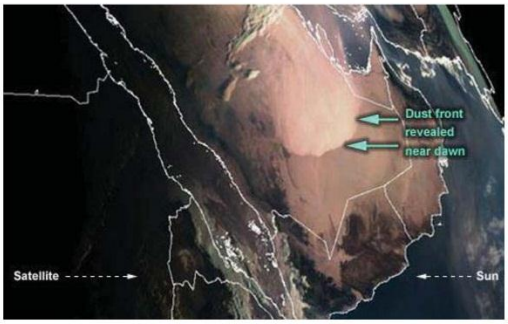

Fig. 1. METEOSAT second generation (MSG) natural color image revealing an advancing dust storm over Saudi Arabia [4].

For Arid and semi-arid areas like Saudi Arabia, Sudan, Libya, etc. which experience DUSA storms, microwave signals will suffer from different weather parameters such as dust particle size and its distribution, visibility, and humidity level during DUSA storms [3]. Since DUSA particles from different regions have different characteristics such as relative permittivity and average dust particle sizes, it has hitherto remained a challenge in creating a generic storm model. Figure 1 reveals a typical dust plume advancing over Saudi Arabia on 20 Feb 2008.

Existing researches have presented several models of this complex phenomenon [5–11]. These models are available at present for estimation of individual impairments, but the methodologies to properly relate these effects together is a challenging task. In [6] the phenomenon of vertical variation of visibility has been discussed, in [5] another approach of adding a vertical path adjustment factor to measure attenuation is presented.

This paper adopts a novel model proposed by the present author; that of a three dimensional relationship of average dust particles size variation with respect to different reference visibilities and heights. It provides

"This work is supported by the Deanship of Scientific Research (DSR) at King Fahd University of Petroleum & Minerals (KFUPM) through project No. FT121006 and FT121013"

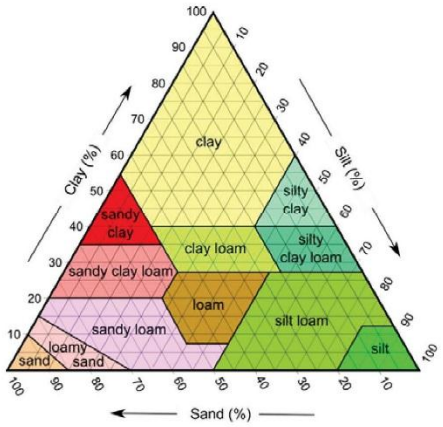

Fig. 2. Triangular diagram of soil texture classes by the United States Department of Agriculture (USDA).

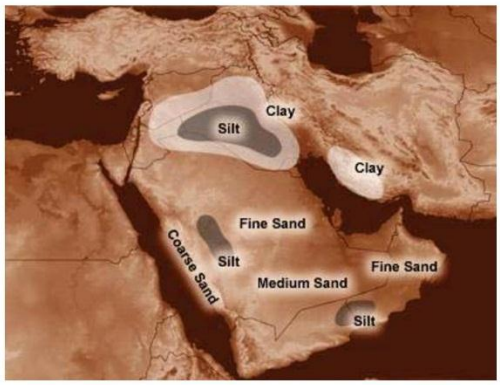

Fig. 3. Map of soil grain types and sizes in the Middle East [4].

a great level of control thus providing dependable and acceptable estimates of dust attenuations for any desired location for non-uniform visibilities, particle size distribution (PSD), various frequency ranges, relative humidity values, and for any selected propagation angle [2]. This would be helpful in optimizing the radio resources and implementing the cost effective link budgets for satellite links while maintaining the end-to-end QoS requirements. This will be demonstrated by redesigning the downlink of a real LEO satellite.

This paper is organized as follows: Section II highlights the most commonly adopted soil taxonomy, and the different dust particles sizes (soil texture). The permittivity of dust particles and how it is affected by relative humidity is presented in Section III. Section IV covers the novel modeling of a dust storm, including the concept of layering and relevant simulations for attenuation. Section V applies the simulated results to a real NanoSat, NIUSAT by introducing the DUSA attenuation parameter in the downlink budget specifications. Section VI is our conclusions and glimpses of our future work.

II. Soil Taxonomy and Physical Description

This section describes the physical description of DUSA storms usually happening in desert areas on earth. Numerous factors can make a region to be prone to DUSA storms including soil type, climate and topography [4]. The PSD is critical in precise prediction of an aftermath of a storm. The soil textural class of the region involved will greatly impact the PSD [3]. The soil texture varies from region to region in the desert areas of the world. The United States Department of Agriculture (USDA) and the National Cooperative Soil Survey (NCSS) developed soil information data based on different soil parameters and characteristics. The triangular diagram in Fig. 2 summarizes the descriptions of the classes.

In Saudi Arabia, DUSA storms are experienced round the year with areas covered by sand and silt which mostly prepare to cause the storms with little extra wind. These types of soils are formed in areas with natural growth of river flood and dry lake-land. Figure 3 shows a map of soil grain sizes in the Arabian Peninsula. Topographically low-lying regions favor DUSA storm generation because prevailing winds are unimpeded by higher terrain. As for climate, it is clear that the world's arid desert and semi-arid climate zones highly correlate with the major deserts [4].

Generally during the storms, top soil is blown up in the air. DUSA with different sizes will stay in the air as long as the wind speed is greater than the speed at which the particles fall down to ground. Larger particles (diameter $> 80\ \mu m$)) rise only few meters and have faster settling speeds once the storm is over. They settle when the winds drop below certain threshold value that is able to carry DUSA particles. Zender [12] did extended work on the issue of gravitational settling for a turbulent mixture of particles. The dust haze, mainly comprising of finer particles (diameter $<\ 20\ \mu m$)), will persist to be airborne for longer periods of time(as there settling speed is very low) at few Km above the ground and downstream from the source for days after the storm, hence greatly impacting earth-satellite communication links [3].

The visibility of a dust storm determines its classification. To be considered as a DUSA storm, the visibility should not exceed 1 Km and below 0.5 Km, it will be considered as severe DUSA storm [13]. A novel technique to determine visibility within the storm will be presented where a layering approach is adopted to divide the DUSA storms into appropriate layers collaborated with the visibility value at different altitudes. This will be elaborated further in the following section.

III. Complex Permittivity and Relative Humidity

DUSA particles in air after a storm make threats to microwave radio systems reliability. Knowledge of the dielectric permittivity of DUSA particles at certain region will be an immense support for better weather impairment estimation in radio communication and radio meteorology [7]. Though several studies exist in literature on the complex permittivity of DUSA samples have been verified, there is no appropriate existing for estimation. Some techniques done recently to estimate the values of the permittivity include resonant cavity measurement, wave guide estimation and extraction results [14].

The permittivity of materials at microwave bands is $\varepsilon = \varepsilon' - j\varepsilon''$, where ε' represents the real part and ε'' represents the imaginary part of the dielectric constant, respectively. A summary of the complex dielectric constants published is shown in Table I. These values are seen to be the most accurate as they have been most cited in literature as per the survey of several geophysical research journals done in [15]. As can be inferred from the table, there is little variation in both real and imaginary parts for the dry soil types as they are dependent on moisture and frequency of operation [7].

In humid weather conditions DUSA particles in air will absorb water vapor. Measurements done by [16] in Khartoum, showed that with 82% relative humidity in air, the dust will absorb up to 5.1% by weight moisture. This has a big impact on the dielectric constant as it increases it considerably. The Arabian Peninsula also experiences such humid conditions especially in the coastal regions. The work done in Khartoum concluded that given any value of air relative humidity (H%), the new dielectric constant can be predicted by (1) and (2) below:

$$\varepsilon'_{\mathrm{H}} = \varepsilon' + 0.04\mathrm{H} - 7.78 \times 10^{-4}\mathrm{H}^2 + 5.56 \times 10^{-6}\mathrm{H}^3 \quad (1)$$

$$\varepsilon''_{\mathrm{H}} = \varepsilon'' + 0.02\mathrm{H} - 3.71 \times 10^{-4}\mathrm{H}^2 + 2.76 \times 10^{-6}\mathrm{H}^3 \quad (2)$$

Where $(\varepsilon' + j\varepsilon'')$ is the dry dust dielectric permittivity.

Experimental studies done by [17] in Riyadh, Saudi Arabia, where they observed and collected data for nine DUSA storms experienced during the year 1987, showed that the measured attenuation is considerably greater than the calculated attenuation using typical sand particles moisture content of up to 10%. They also proposed that moisture gained by dust particles will reach maximum of 10% for a relative humidity of 90%.

We can conclude that moist DUSA particles will affect the satellite microwave links more severely than dry particles in humid regions and thus relative humidity is a necessary parameter in accurate determination of satellite links degradation caused by meteorological factors.

A recent work by the present author in [18] presented an analytical solution to predict gaseous attenuation (GA) in dust free environments. GA was calculated by summing the effects of all of the significant resonance lines of the gasses in air (most dominantly those from atmospheric oxygen and water vapor). We do not consider it in this work as we focus more on the effect of dusty environment on the satellite links.

TABLE I
Summary of published DUSA Complex Permittivities.

Band	Frequency Range (GHz)	Soil Type	Moisture Content %(g H_2O/g)	Dielectric Constant $\varepsilon' - j\varepsilon''$	Reported by
S	1 - 4	Sandy Soil	0	2.55-j0.016	Von Hippel [19]
			4	4.4-j0.2024	
			16.8	20-j2.6	
		Loamy	0	2.44-j0.003	
			2.2	3.5-j0.14	
			13.7	20-j2.4	
		Clay	0	2.20-j0.034	
			20	11.3-j2.825	
X	8 - 12	Sandy Soil	0	2.53-j0.01	Von Hippel [19]
			3.88	3.6-j0.432	
			16.8	13-j3.77	
		Loamy	0	2.44-j0.003	
			13.7	13.8-j2.484	
Ku	12 - 18	Sandy Soil	0.3	2.8-j0.035	Njoku and Kong [20]
			5	3.9-j0.62	
			10	5.5-j1.3	
			20	9.2-j4	
			30	11.8-j7	
K	18 - 26.5	Silty Clay Loam	3	3.4-j0.2	Schmugge, Gloersen, Wilheit and Geiger [21]
			12	4.7-j1.1	
			22	13.6-j6.8	
			30	16.25-j9.25	
Ka	26.5 - 37	Sandy Soil	0.3	2.5-j0.028	Njoku and Kong [20]
			5	3.6-j0.65	
			10	5.1-j1.4	
			20	7.8-j5.3	
			30	9.8-j9.9	
		Loamy Fine Sand	0	2.53 - j0.065	Geiger and Williams [22]
			5	2.45-j0.375	
			10	4-j1.325	
			15	6.72-j3.188	
			20	7.375-j4.156	
		Sandy Clay Loam	0	2.515-j0.073	
			5	2.88-j0.353	
			10	3.290-j0.728	
			15	7.088-j3.5	
			20	8.588-j4.765	

IV. Dust Storm Modeling

In this section a novel approach to model the DUSA storms described in section II is presented and methods to get precise attenuation measurements have been defined. Based on the knowledge of two dimensional (side and top view) models of dust storm discussed in [5], we present a three dimensional Dust Storm model as shown in Fig. 4.

A. Layering Concept and Visibility

Intensity of dust storm plumes is not uniform, it varies on both horizontal and vertical expanses, being highest in the middle and lowering around the horizontal start, end and vertical edges. It contains several layers while moving from the base in vertical direction till top. These layers represent different levels of visibility based on non-uniform particle size and intensity distributions within the DUSA. The particles size distribution is similar to an exponentially decaying function where the base layer contains heavier and denser particles leading to more attenuation whereas as we move in vertical direction their size and density reduces which constitute lesser attenuation. The same phenomenon is true as we move horizon-

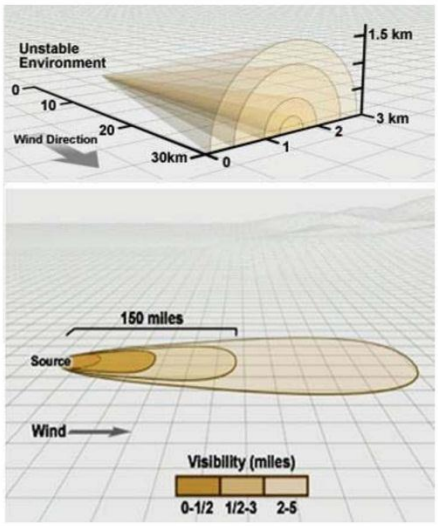

Fig. 4. Top - $3-D$ Schematic of a dust plume geometry. Bottom - Typical distribution of visibility within a dust storm on the horizontal expanse [4].

tally away from the storm's epicenter. Visibility starts from zero level at the source regions and increase gradually as propagation travel far away from its origin. Thus, for a given DUSA storm of around 240 Km wide, visibility can range from 0.5 Km to around 5 Km [4]. Both the vertical and horizontal expanses can be seen in Fig. 4 where the lighter colors indicate increased visibility.

In this paper, we model the visibility in the storm by considering the layering on the vertical expanse only. The storm is chopped off into layers based on a concept of doubling visibility from the starting point of that layer [2]. To achieve more precision we can make the visibility windows narrower, but on the other hand this precision would be dependent on our computational cost. Equation (3) can be used in a recursive manner to make the visibility based layers in dust storm [4]:

$$\mathrm{h_i} = \mathrm{h_{(i-1)}} \left[\frac{\mathrm{V_i}}{\mathrm{V_{(i-1)}}} \right]^{3.85}, \tag{3}$$

where $h_{(i-1)}$ and $V_{(i-1)}$ are the reference height and visibility respectively, and i indicates the different dust layers. Equation (3) can be mathematically re-adjusted to find various levels of visibility depending upon different heights:

$$\mathrm{V_i} = \mathrm{V_0} \left[\frac{\mathrm{h_i}}{\mathrm{h_{(i-1)}}} \right]^{0.26}. \tag{4}$$

Similarly, by generalizing the concept of [11] the total Slant Path (L) traversed by microwave signals in the dust storm is broken into smaller patches based on different levels of visibility at each layer, as follows:

$$\mathrm{L}(\theta) = \mathrm{L_1} + \mathrm{L_2} + \cdots + \mathrm{L_N} = \frac{\sum_{\mathrm{i}}^{N} \mathrm{h_i}}{\sin\theta}, \tag{5}$$

where θ is the elevation angle and N is the total number of layers.

B. Non-Uniform Dust Distribution

Dust PSD assessment is very important for predicting effects of dust storms. Each dust storm may have totally uncorrelated dust distributions; moreover this distribution is also dependent on height. As the height decreases the particles average diameter increases because the heavier dust particles have greater fall velocities as compared to the particles with smaller size that remain suspended in air for longer intervals of time. For all the samples the relation among average diameter (D_{av} μm), reference diameter (D_0 μm), and height (h $meters$) can be represented by:

$$\mathrm{D_{av}} = \mathrm{D_0} \,.\, \mathrm{h}^{-\alpha}, \tag{6}$$

where $\alpha = 0.155$. If we combine (3) and (6), then after simplification we get another expression for computing the values of average diameter of DUSA particles at several reference heights and visibilities [3]:

$$\mathrm{D_{av}(h,V)} = \left[\frac{\mathrm{D_o}}{\mathrm{h_0^{\alpha}}} \right] \left[\frac{\mathrm{V_0}}{\mathrm{V}} \right]^{0.596}, \tag{7}$$

where V is visibility in Km, D_0, h_0 and V_0 are the reference diameter, height and visibility, respectively. We have incorporated Freeman's Chain Code algorithm in averaging the dust particles sizes for better estimates. Assuming an approximate circular geometry for the dust particles, we can compute the equivalent or average DUSA particles radius from (7) as:

$$\mathrm{r_e} = \mathrm{D_{av}}/2 \tag{8}$$

C. Dust Attenuation Modeling

Each layer constitutes its specific point attenuation on the microwave signal depending on the measure of visibility as well as the equivalent dust particles radii. These individual layered attenuations are then summed up reaching the end of dust storm which can be discovered by attaining certain lower bound of visibility comparable to visibility in free space [2]. The DUSA attenuation is extracted from the following equations:

$$\mathrm{A_{Pi}} = \left[\frac{567}{\mathrm{V\ r_e^2}\ \lambda} \right] \left[\frac{\varepsilon''}{(\varepsilon'+2)^2 + \varepsilon''^2} \right] \sum_{\mathrm{i}}^{\mathrm{N}} \mathrm{p_i r_i^3} \tag{9}$$

$$\mathrm{A_D} = \sum_{\mathrm{i}}^{\mathrm{N}} \mathrm{Ap_i}, \tag{10}$$

where A_P and A_D are the point and total attenuations, respectively.

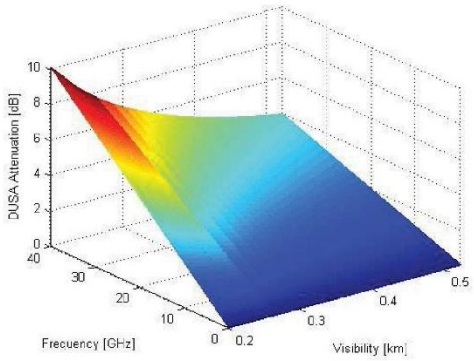

Fig. 5. Simulation result of the total DUSA attenuation.

r_e is the average DUSA particle radius.
λ is the Wavelength.
$\sum_{i}^{N} p_i r_i^3$ represents the summation of the probability particle size between r_i series of particle volume.

In our case, we have taken into account a range of visibilities, frequencies and several particles sizes along with altitude dependent distributions for all the DUSA particles sizes to compute respective point attenuations as shown in Fig. 5. Also, listing values of dielectric constants at different levels of humidities and frequencies is as summarized in Table I. These data will be immensely useful to support budgeting of real operational satellite parameters at any given location. The next section demonstrates exactly that by re-designing the downlink budget of a NanoSat named NIUSAT. The dust storm modeling parameters used comprised a storm height of 5 Km in the Eastern region of Saudi Arabia mainly composed of a turbulent clay and silt mixture having a moisture content of 4%.

V. Application Example - Effective Downlink Budget for LEO Satellites

A. NIUSAT Introduction

NIUSAT is a Nano satellite designed and developed by the Higher Education of Noorul-Islam University in India. It has a Miniature Wide Field Sensor (MWiFS) for agriculture and disaster management support applications. The satellite images captured through color discrimination will be used for determining agricultural diseases in the crops and plantations. It is also going to provide a much needed timely assistance for disaster management support systems. Another interesting application include detecting fish rich regions in the oceans [23].

NIUSAT is planned to be operational in the near future. It will be at the polar sun synchronous orbit operating at LEO altitudes of 560-880 Km at an orbital angle inclination of 97°-99°. Its orbital period is expected to be 96-100 min. An estimated 225,000 Km^2 will be covered by the NanoSat. The downlink which is of concern will be operated at 2.24 GHz at the S-Band. Further link specifications can be inferred from Table II which constitute the input parameters to the simulation.

TABLE II
Link Specifications and Input Parameters [23]

Downlink Operating Frequency [GHz]	2.24
Transmitted Power [W]	0.5
Transmitting Antenna Gain [dBi]	5 (Minimum available)
Diameter of the Parabolic Antenna (Ground station)	1.3m
Aperture efficiency of Parabolic Reflector	0.55 (Minimum available)
Distance between Satellite and Ground Station (Km)	900
Ground Station Receiver Noise [K]	119 (Approximate)
Ground Station Antenna Noise [K]	35 (Approximate)
Ground Station Amplifier Noise [K]	60 (Approximate)
Bit Rate of the data (Mbps)	1
Bit Error Rate (BER)	10^{-6}
Modulation	QPSK

TABLE III
Considered LEO Losses (Maximum Values)

Atmospheric Loss (dB)	1
Rain Attenuation (dB)	0.5
Fog Attenuation (dB)	0.03
Snow Attenuation (dB)	0.01
Atmospheric Reflection (dB)	0.2
Ionospheric Loss (dB)	0.6
Polarization Loss (dB)	0.3
DUSA Attenuation (dB)	**0.6254**

B. An Effective Downlink Budget

Details of the downlink budget calculation can be found in [23]. Several other losses have been considered with their maximum values at LEO to ensure an efficacious link margin. For the first time in this paper, we introduce DUSA attenuation in the downlink budget specifications. The value was extracted from the simulations in the previous section. A maximum estimated value of 0.6254 dB, is shown in Table III along with all other losses. Finally the link budget is redesigned with DUSA attenuation considered. The output parameters are shown in Table IV. The link margin is an important parameter in satellite links and represents the difference between the available and the required value of the energy-to-noise ratio. It can be viewed as the amount by which the received power exceeds the receiver sensitivity. In a perfect telecommunication channel this difference should not be there (i.e. zero). According to the recommendations of the ITU-R (Rec. UIT-R F.1247-1), practical satellite-earth links must maintain a healthy link margin between 2-4 dB in order to have effective communication links with acceptable QoS. As can be inferred from the output parameters, the NIUSAT's link margin is found to be 3.0761 dB which is sufficiently

TABLE IV
SUMMARY OF DOWNLINK OUTPUT PARAMETERS

Effective Isotropic Radiated Power (dBW)	1.9897
Free Space Path Loss (dB)	158.5398
Total Losses (dB)	161.7652
Received Power (dB)	-132.7652
Noise Density (dB)	-207.1389
Received Power to Noise Ratio (dB)	74.3736
Energy to Noise Ration (Available) (dB)	14.3736
Energy to Noise Ration (Required) (dB)	11.2975
Link Margin (dB)	**3.0761**

healthy for a reliable satellite communication link.

VI. Conclusions and Future Work

Since dust storms are a significant meteorological phenomenon increasingly occurring in arid and semi-arid regions of the world, mitigation techniques of satellite-earth channel fading are crucial to maintain certain levels of QoS. This can be done by swiftly changing link parameters to adapt to any meteorological impairment. The shorter wavelengths at high frequencies are most affected, thus DUSA attenuations should not be neglected if efficient communications links are to be designed.

The dust storm model adopted proved to have a great level of control in providing dependable and acceptable estimates of dust attenuations for any desired location according to different visibilities, dust PSD, various frequencies, relative humidity values, and elevation angles.

DUSA attenuation was introduced for the first time in the effective link budget design of the soon to be launched NanoSat, NIUSAT. The link margin was found to be in a healthy and adequate region supporting with reasonable results in terms of effective cost of operation and design.

Future work is in progress to model the visibility in a dust storm by taking into account the gradual variations in both the horizontal and vertical expanses forming a near perfect $3-D$ look-alike of a DUSA plume.

ACKNOWLEDGEMENT

The authors wish to thank King Fahd University of Petroleum and Minerals (KFUPM) presented by the Electrical Engineering (EE) department for supporting this project and for facilitating the logistics needed for installing satellite system and collecting data.

References

[1] C. S. Bristow, K. A. Hudson-Edwards, and A. Chappell, "Fertilizing the amazon and equatorial atlantic with west african dust," *Geophysical Research Letters*, vol. 37, no. 14, p. L14807, 2010.

[2] K. Harb, B. Omair, S. Abdul-Jauwad, A. Al-Yami, and A. A. Al-Yami, "A proposed method for dust and sand storms effect on satellite communication networks," in Innovations on Communication Theory INCT, (Istanbul, Turkey), pp. 33–37, Oct. 2012.

[3] K. Afzaal, T. K. Bandopadhyaya, and S. Poonam, "Effect of soil textural class and relative humidity of regions in accurate prediction of attenuation of millimeter waves during sand and dust storms," *The Fourth International Kharkov Symposium on Physics and Engineering of Millimeter and Sub-Millimeter Waves.*, vol. 1, pp. 393–395, 2001.

[4] The-COMET-Program, "Atmospheric dust module." website: http://www.meted.ucar.edu/eumetsat/at_dust/, last accessed date Feb. 2014.

[5] J. Goldhirsh, "Attenuation and backscatter from a derived two-dimensional duststorm model," *IEEE Transactions Antennas Propagation*, vol. 49, no. 12, pp. 1703–1711, 2001.

[6] S. O. Bashir and N. J. McEwan, "Microwave propagation in dust storms: A review," *in Proc. Inst. Elect. Eng.*, vol. 133, pp. 241–247, June 1986.

[7] S. I. Ghobrial and S. M. Sharief, "Microwave attenuation and cross polarization in dust storms," *IEEE Trans. Antennas Propagat.*, vol. AP-35, pp. 418–425, April 1987.

[8] E. A. A. Elsheikh, M. R. Islam, A. H. M. Z. Alam, A. F. Ismail, K. Al-Khateeb, and Z. Elabdin, *The Effect of Particle Size Distributions on Dust Storm Attenuation Prediction for Microwave Propagation.* Kuala Lumpur, Malaysia, DOI: 10.1109/ICCCE.2010.5556831, May 2010.

[9] Z. E. O. Elshaikh, M. R. Islam, O. O. Khalifa, and H. E. Abd-El-Raouf, "Mathematical model for the prediction of microwave signal attenuation due to duststorm," *Progress In Electromagnetics Research M*, vol. 6, pp. 139–153, 2009.

[10] Z. Elabdin and M. Islam, *Duststorm Measurements for the Prediction of Attenuation on Microwave Signals in Sudan.* Kuala Lumpur, Malaysia, 2008.

[11] E. A. A. Elsheikh, M. R. Islam, K. Al-Khateeb, A. Z. Alam, and Z. O.Elshaikh, "A proposed vertical path adjustment factor for dust storm attenuation prediction," in *4th International Conference on Mechatronics ICOM*, (Kuala Lumpur, Malaysia), May 2011.

[12] C. S. Zender, H. Bian, and D. Newman, "Mineral dust entrainment and deposition (DEAD) model: Description and 1990s dust climatology," *Journal of Geophysical Research: Atmospheres (19842012)*, vol. 108, no. D14, pp. 1984–2012, 2003.

[13] R. E. Hushcke, *Ed., Glossary of Meteorology.* Boston, MA: Amer. Meteorological Soc., 1995.

[14] X.-Y. Dong, H.-Y. Chen, and D.-H. Guo, "Microwave and millimeter-wave attenuation in sand and dust storms," *Antennas and Wireless Propagation Letters, IEEE*, vol. 10, pp. 469–471, 2011.

[15] A. Ansari and B. G. Evans, "Microwave propagation in sand and dust storms," in *IEE Proceedings F (Communications, Radar and Signal Processing)*, vol. 129, pp. 315–322, IET, 1982.

[16] S. Sharif, "Chemical and mineral composition of dust and its effect on the dielectric constant," *Geoscience and Remote Sensing, IEEE Transactions on*, vol. 33, pp. 353–359, March 1995.

[17] M. A. Alhaider and A. A. Ali, "Experimental studies on millimeterwave and infrared propagation in arid land: The effect of sand storms," in *Antennas and Propagation, 1989. ICAP 89., Sixth International Conference on (Conf. Publ. No. 301)*, pp. 268–270, IET, 1989.

[18] K. Harb, O. Butt, S. Abdul-Jauwad, and A. M. Al-Yami, "Systems adaptation for satellite signal under dust, sand and gaseous attenuations," *Journal of Wireless Networking and Communications*, vol. 3, no. 3, pp. 39–49, 2013.

[19] A. R. V. Hippel, *Dielectric Materials and Applications.* Cambridge, MA: MIT Press, 1954.

[20] E. G. Njoku and J.-A. Kong, "Theory for passive microwave remote sensing of near-surface soil moisture," *Journal of Geophysical Research*, vol. 82, no. 20, pp. 3108–3118, 1977.

[21] T. Schmugge, P. Gloersen, T. Wilheit, and F. Geiger, "Remote sensing of soil moisture with microwave radiometers," *Journal of Geophysical Research*, vol. 79, no. 2, pp. 317–323, 1974.

[22] F. E. Geiger and D. Williams, "Dielectric constants of soils at microwave frequencies," *NASA Tech. Rep. TMS-65987. Washington, DC*, 1972.

[23] A. Arun and T. K. Sreeja, "An effective downlink budget for 2.24 GHz s-band LEO satellites," in *Information & Communication Technologies (ICT), 2013 IEEE Conference on*, pp. 342–345, 2013.